

REST-FRAME ULTRAVIOLET SPECTRA OF $Z \sim 3$ LYMAN BREAK GALAXIES¹ALICE E. SHAPLEY AND CHARLES C. STEIDEL²
California Institute of Technology, MS 105–24, Pasadena, CA 91125MAX PETTINI
Institute of Astronomy, Madingley Road, Cambridge UKKURT L. ADELBERGER³
Harvard-Smithsonian Center for Astrophysics, 60 Garden St., Cambridge, MA 02139
Draft version October 25, 2018

ABSTRACT

We present the results of a systematic study of the rest-frame UV spectroscopic properties of Lyman Break Galaxies (LBGs). The database of almost 1000 LBG spectra proves useful for constructing high S/N composite spectra. The composite spectrum of the entire sample reveals a wealth of features attributable to hot stars, H II regions, dust, and outflowing neutral and ionized gas. By grouping the database according to galaxy parameters such as Ly α equivalent width, UV spectral slope, and interstellar kinematics, we isolate some of the major trends in LBG spectra which are least compromised by selection effects. We find that LBGs with stronger Ly α emission have bluer UV continua, weaker low-ionization interstellar absorption lines, smaller kinematic offsets between Ly α and the interstellar absorption lines, and lower star-formation rates. There is a decoupling between the dependence of low- and high-ionization outflow features on other spectral properties. Additionally, galaxies with rest-frame $W_{Ly\alpha} \geq 20$ Å in emission have weaker than average high-ionization lines, and nebular emission lines which are significantly stronger than in the sample as a whole. Most of the above trends can be explained in terms of the properties of the large-scale outflows seen in LBGs. According to this scenario, the appearance of LBG spectra is determined by a combination of the covering fraction of outflowing neutral gas which contains dust, and the range of velocities over which this gas is absorbing. In contrast, the strengths of collisionally excited nebular emission lines should not be affected by the nature of the outflow, and variations in these lines may indicate differences in the temperatures and metallicities in H II regions of galaxies with very strong Ly α emission. Higher sensitivity and spectral resolution observations are still required for a full understanding of the covering fraction and velocity dispersion of the outflowing neutral gas in LBGs, and its relationship to the escape fraction of Lyman continuum radiation in galaxies at $z \sim 3$.

Subject headings: galaxies: active — galaxies: nuclei — galaxies: evolution — quasars: general — galaxies: high-redshift

1. INTRODUCTION

Until now, the rest-frame UV spectra of Lyman Break Galaxies (LBGs) have been used primarily to measure redshifts. At first, the spectra were used to confirm the cosmologically distant nature of galaxies photometrically selected with the Lyman Break Technique to be at $z \sim 3$ (Steidel et al. 1996a,b; Lowenthal et al. 1997). Spectroscopic redshifts were also necessary to study the large-scale spatial distribution and clustering properties of LBGs (Adelberger et al. 1998; Steidel et al. 1998; Giavalisco et al. 1998). Furthermore, the determination of the $z \sim 3$ rest-frame UV luminosity function required knowledge of the redshifts of LBGs, combined with the optical apparent magnitudes and colors (Steidel et al. 1999). Most recently, the redshifts measured from rest-frame UV spectra have been used to study the cross-correlation of the large-scale distributions of galaxies and the inter-galactic medium within the same cosmic volume (Adelberger et al. 2002a). Given the faint nature of LBGs (most have $\mathcal{R}_{AB} = 24-25.5$), the desire to observe a large sample results in individual spectra with low signal-to-noise (S/N) ratios and spectral resolution. In most cases, the

low S/N of LBG spectra precludes any analysis more detailed than the determination of redshifts.

One notable exception is the galaxy MS1512-cB58, an L^* LBG at $z = 2.73$ with an apparent magnitude of $V = 20.6$ due to lensing by a foreground cluster at $z = 0.37$ (Yee et al. 1996). Cluster lensing boosts the apparent luminosity of cB58 by a factor of ~ 30 , enabling relatively high-resolution ($R \simeq 5000$) studies of its rest-frame UV spectrum (Pettini et al. 2000, 2002). The velocity profiles of low and high-ionization interstellar metal absorption features have been characterized in detail; the weakest interstellar metal transitions have been used together with the damped Ly α absorption profile to determine the abundance pattern in cB58 (an α /Fe enhancement indicative of a young stellar population, and an abundance of $\sim 0.4Z_{\odot}$ for the α elements); C IV and Si IV P-Cygni stellar wind profiles have been used as independent probes of the stellar population and metallicity; weak stellar absorption features have been used to precisely measure the systemic velocity of the stars, relative to which the redshifts of Ly α emission and interstellar absorption indicate offsets of several hundred km s⁻¹; finally, the

¹ Based, in part, on data obtained at the W.M. Keck Observatory, which is operated as a scientific partnership among the California Institute of Technology, the University of California, and NASA, and was made possible by the generous financial support of the W.M. Keck Foundation.

² Packard Fellow

³ Harvard Society Junior Fellow

strengths of the strongest interstellar absorption features (which have zero transmission at line center) have been used to infer a high covering fraction of outflowing neutral material, through which negligible Lyman continuum emission can escape. For the vast majority of unlensed LBGs, it is unfortunately not possible to obtain individual spectra which contain the same high-quality information about physical conditions. Since cB58 is only one object, we need to worry about how “typical” its continuum and spectroscopic properties are, relative to the range seen in the entire sample of LBGs.

Even from the low S/N spectra used to measure redshifts, we discern a large variation in the types of spectra associated with LBGs. Most obviously, there are large ranges of Ly α profile shapes and UV continuum slopes. There are also variations among the equivalent widths of the few strong interstellar absorption lines which we detect most of the time in individual spectra, and of the redshift offset measured between Ly α emission and interstellar absorption (for spectra in which both types of features are detected). While there is no hope of collecting data of comparable quality to the cB58 spectra for individual unlensed LBGs, we have assembled a sample of almost 1000 spectroscopically confirmed $z \sim 3$ galaxies over the past six years. By dividing our spectroscopic database into subsamples according to specific criteria, and creating high S/N composite spectra of each subsample, we hope to understand how the LBG spectroscopic properties depend in a systematic way on other galaxy properties.

Past uses of composite LBG spectra have proven very illustrative. For example, a composite of 29 individual LBG spectra at $\langle z \rangle = 3.4 \pm 0.09$ shows significant residual flux shortward of the Lyman limit at 912 Å (Steidel, Pettini, & Adelberger 2001). If this composite spectrum is taken to be representative of LBGs at $z \sim 3$, the LBG contribution to the ionizing background could exceed that of QSOs at similar redshifts by as much as a factor of 5. The appearance of this composite spectrum is very different from that of cB58, with strong Ly α emission, a continuum slope in the bluest quartile of the total LBG sample, and interstellar absorption lines roughly half the strength of those in the cB58 spectrum. Determining the relative numbers of LBGs that resemble this composite versus those that more closely resemble cB58 is important for determining the overall contribution of LBGs to the ionizing background. Composite LBG spectra were also constructed for galaxy subsamples grouped by the stellar population age inferred from optical/near-IR photometry (Shapley et al. 2001). The “young” ($t \leq 35$ Myr) and “old” ($t \sim 1$ Gyr) composite spectra exhibited systematic differences, including significantly stronger Ly α emission in the “old” spectrum, and stronger interstellar absorption and stellar P-Cygni wind features in the “young” spectrum. Such differences may indicate an evolutionary sequence for the appearance of the rest-frame UV spectra.

Based on the promise of these specific composite studies, we are motivated to undertake a more general study of the spectroscopic properties of the entire LBG sample. This systematic study is in some ways a high-redshift analog to the work of Heckman et al. (1998), which characterized the region of UV spectroscopic parameter space inhabited by local starburst galaxies. In particular, we would like to gain more detailed information about the properties of the large-scale outflows of interstellar material which are inferred in LBGs from blueshifted interstellar absorption and redshifted Ly α emission, relative to the systemic stellar redshift (Pettini et al. 2001, 2002; Franx

et al. 1997; Lowenthal et al. 1997). The outflows represent not only an important feedback process which affects galaxy formation and evolution, but also may have a profound impact on the metal enrichment, ionization, and physical state of the surrounding intergalactic medium (Adelberger et al. 2002a,b; Adelberger 2002a; Steidel, Pettini, & Adelberger 2001). So far, most of the information about the nature of outflows at high redshift comes from high-quality observations of a single galaxy – cB58 – and from studies of the metal content and HI opacity of the Ly α forest near LBGs. The current survey provides information which is complementary to both types of observations, as it explores outflow properties from the galaxy perspective, but is based on a much larger (if lower spectral resolution) sample of galaxies.

The LBG spectroscopic sample is described in §2, while §3 presents the method of generating composite spectra and defining the “rest-frame” in the presence of large-scale velocity fields. §4 gives an overview of the types of stellar and interstellar spectroscopic features which appear in high S/N composite LBG spectra, *some of which have not previously been observed in UV spectra of local star-forming regions*. In §5, we present some of the important trends observed in LBG spectra, with particular attention to outflow-related properties. Finally, in §6 we present a physical picture which is broadly consistent with the observations, and highlight the need for several future observations to test this picture.

2. THE LBG SPECTROSCOPIC SAMPLE

The individual galaxy spectra used to construct the composite spectra in this paper were drawn from the Lyman Break Galaxy (LBG) survey of $z \sim 3$ galaxies. The details of our survey have been presented elsewhere (Steidel et al. 1996a,b, 1999) and will be extensively summarized in a future work (Steidel et al. 2003, in preparation), so here we present only a few relevant features. The full LBG photometric sample consists of 2347 galaxies in 17 separate fields with optical colors satisfying the following criteria:

$$\mathcal{R} \leq 25.5, \quad G - \mathcal{R} \leq 1.2, \quad U_n - G \geq G - \mathcal{R} + 1 \quad (1)$$

plus an additional 180 galaxies with the same color criteria, but \mathcal{R} magnitudes which are as faint as $\mathcal{R} = 26$ (which are located in the LBG survey field containing the bright quasar, Q1422+239, for which we obtained significantly deeper photometry, allowing an extension of the LBG selection technique to fainter magnitudes).

We have spectroscopically observed 1320 of these photometric candidates using the Low Resolution Imaging Spectrometer (LRIS) at the W.M. Keck Observatory (Oke et al. 1995). Most of the spectra were obtained using a 300 lines mm⁻¹ grating blazed at 5000 Å, and a multi-object slit mask with 1''/4 slits, providing a spectral resolution of 8–12 Å, depending on the seeing. Recent spectroscopic data, including some of the observations in the Q0933+288 and Q1422+2309 fields, and all of the data in the Q0302–003 field, were obtained with the new blue arm of LRIS (LRIS-B; McCarthy et al. 1998; Steidel et al. 2003), and dispersed by a 300 lines mm⁻¹ grism blazed at 5000 Å. This setup provided slightly higher spectral resolution than the 300-line grating setup, and much higher throughput. Typical exposure times for both setups were 3×1800 sec with 1''/0 dithers between exposures to provide for adequate sky-subtraction. The two-dimensional, sky-subtracted, and coadded spectra were then extracted to one-dimension, and wavelength

calibrated using a HgNeAr arc-lamp spectrum. Spectra were flux-calibrated with observations of standard stars taken close to the time of the science observations. Finally, air wavelengths were converted to vacuum wavelengths, in order to measure redshifts in the vacuum frame. The average S/N ratio of spectra in the sample is ~ 4 per resolution element.

From this sample of spectra, we identify 36 stars, 2 absorption-line galaxies at $z \sim 0.5$, 2 galaxies with $z \simeq 1.98$, 957 objects at $z > 2$, and 292 objects for which we cannot measure a redshift. Of the 957 galaxies at $z > 2$, 12 are identified as broad-lined AGN due to the presence of emission lines with $\text{FWHM} > 2000 \text{ km s}^{-1}$, while 16 are identified as narrow-lined AGN with strong $\text{Ly}\alpha$ emission accompanied by significant C IV $\lambda 1549$ emission, but $\text{FWHM} < 2000 \text{ km s}^{-1}$ (Steidel et al. 2002). We exclude from the spectroscopic sample the 28 objects identified as AGN on an individual basis (though we may have included galaxies with low-level AGN activity which is undetected in individual spectra but may become evident in the composites. We will treat this point further in section 4.3.1). Furthermore, we include only galaxies whose redshifts were independently and securely confirmed by at least two members of our group. This last criterion limits our composite sample to 811 spectra.

3. GENERATING THE COMPOSITE SPECTRA

There are several steps required to generate the composite galaxy spectra presented in this work. The first step consists of carefully defining a sample of galaxy spectra to be combined. Each extracted, one-dimensional, flux-calibrated spectrum in the sample is then shifted into the rest frame. The spectra are then averaged, after being scaled to a common mode in the wavelength range 1250-1500 \AA and rebinned to a common dispersion of 1 \AA per pixel. In order to exclude both positive and negative sky subtraction residuals and cosmic ray events, an equal number of positive and negative outliers are rejected at each dispersion pixel, totaling less than 10% of the data.

3.1. Measuring Redshifts

One of the non-trivial aspects of generating the composite spectra consists of defining a systemic rest frame for each galaxy. The low S/N ratio of typical LBG spectra precludes much more than measuring redshifts from the very strongest rest-frame UV features. These features include H I $\text{Ly}\alpha$, seen either in emission, absorption, or a combination of both; low-ionization resonance interstellar metal lines such as Si II $\lambda 1260$, O I $\lambda 1302 + \text{Si II } \lambda 1304$, C II $\lambda 1334$, Si II $\lambda 1526$, Fe II $\lambda 1608$, and Al II $\lambda 1670$, which are associated with the neutral interstellar medium; and high-ionization metal lines such as Si IV $\lambda \lambda 1393, 1402$ and C IV $\lambda \lambda 1548, 1550$ associated with ionized interstellar gas and P-Cygni stellar wind features. In 28% of the rest-frame UV LBG spectra in our spectroscopic sample, the only spectral feature visible is $\text{Ly}\alpha$ emission. In 32% of the spectra, $\text{Ly}\alpha$ appears only as broad absorption, and multiple low- and/or high- ionization interstellar absorption lines are used to measure the redshift (broad $\text{Ly}\alpha$ absorption is not very precise as a redshift indicator). Finally, in the remaining 40% of the spectra, both $\text{Ly}\alpha$ emission and interstellar absorption lines are visible and both can be used to measure redshifts. In 95% of the cases where both $\text{Ly}\alpha$ emission and interstellar absorption lines have been used to measure the redshift of the galaxy, the $\text{Ly}\alpha$ emission redshift is higher than the interstellar absorption redshift. Figure 1 shows the distribution of $\Delta v_{\text{em-abs}}$, which

has $\langle \Delta v_{\text{em-abs}} \rangle \sim 650 \text{ km s}^{-1}$. This velocity difference indicates that at least one of the two sets of features is not at rest with respect to the stars in the galaxy. Such kinematics suggest that LBGs are experiencing large-scale outflows caused by the mechanical energy input from supernova explosions which are the result of vigorous massive star-formation rates. It has been shown that, in the local universe, any galaxy with a star-formation rate surface-density $\Sigma_* \geq 0.1 M_\odot \text{ yr}^{-1} \text{ kpc}^{-2}$ is capable of driving a superwind (Heckman 2002). Given their typical star-formation rates and physical sizes, LBGs easily satisfy and exceed the criteria for driving a superwind (Shapley et al. 2001; Giavalisco, Steidel, & Macchetto 1996b).

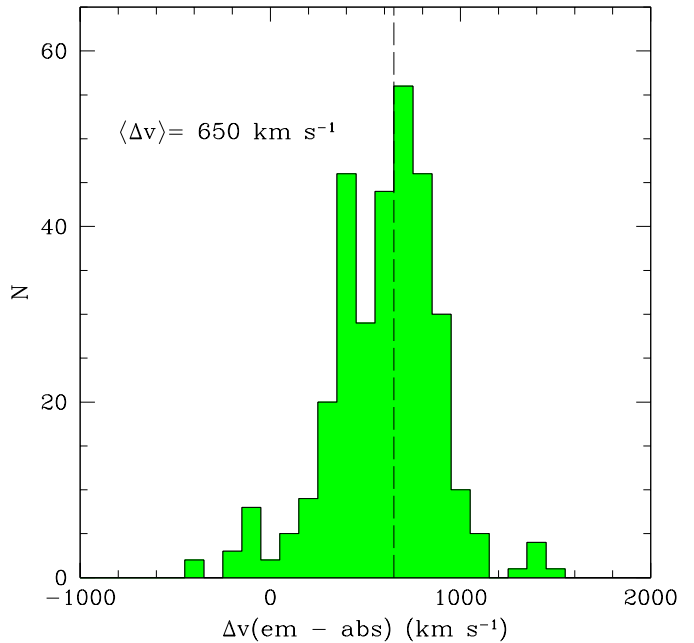


FIG. 1.— The distribution of velocity offsets between $\text{Ly}\alpha$ emission and low-ionization interstellar absorption. The most straightforward indication that LBGs are experiencing large-scale outflows of their interstellar material is the velocity offset measured in individual spectra between $\text{Ly}\alpha$ emission and interstellar absorption lines. This histogram shows the distribution of velocity offsets for the 323 galaxies with spectra in which both types of features are detected. The mean velocity offset (redshift difference) is $\Delta v = 650 \text{ km s}^{-1}$ ($\Delta z = 0.008$).

Since the only features which can be detected in individual LBG spectra seem to trace outflow kinematics, the outflows complicate our effort to assign systemic redshifts. In general, stellar systemic redshifts cannot be measured for individual galaxies because UV photospheric features from hot stars are much too weak to see in typical LBG spectra. In order to estimate stellar systemic redshifts for individual galaxies, we applied the formulae presented in Adelberger et al. (2002a), which predict a value of the systemic redshift for three separate cases: when there is only a $\text{Ly}\alpha$ emission redshift; when there is only an interstellar absorption redshift; and when there are both $\text{Ly}\alpha$ emission and interstellar absorption redshifts.

While no reference was made to stellar photospheric features in the estimate of the systemic redshifts of individual galaxies, the rest-frame composite spectrum presented in the next section indicates a mean systemic velocity of $\Delta v = -10 \pm 35 \text{ km s}^{-1}$ for the three strongest stellar features, which we have identi-

fied as C III $\lambda 1176$, O IV $\lambda 1343$, and S V $\lambda 1501$.⁴ It is worth noting possible contributions to the O IV $\lambda 1343$ absorption from Si III $\lambda 1341$, and to the S V $\lambda 1501$ absorption from Si III $\lambda 1501$, if there is a significant B-star component in the composite spectrum. However, at least the Si III $\lambda 1501$ contribution will not change the inferred negligible systemic velocity of the feature which we have identified as S V $\lambda 1501$. The insignificant velocities of the stellar features demonstrate the success of the systemic redshift estimates for the LBGs included in composite spectra, at least on average. Also, since the stellar features appear at roughly zero velocity, the redshifts and blueshifts of other sets of spectral features measured relative to the rest-frame of the composite spectrum should offer a true representation of the average kinematic properties of the large-scale galactic outflows in LBGs. The establishment of the velocity zeropoint from the stellar lines in composite spectra represents a significant improvement over the kinematic information contained in individual rest-frame UV spectra, where only the strongest interstellar outflow-related features are detected.

4. LBG REST-FRAME UV SPECTROSCOPIC FEATURES

Figure 2 shows a composite spectrum which is the average of our entire spectroscopic sample of 811 LBGs, combined in the manner described in section 3. Rest-frame UV spectra of LBGs are dominated by the emission from O and B stars with masses higher than $10M_{\odot}$ and $T \geq 25000K$. The overall shape of the UV spectrum is modified by dust extinction internal to the galaxy, and, at rest wavelengths shorter than 1216 \AA , by inter-galactic HI absorption along the line of sight. Composite spectra contain the average of many different lines of sight through the IGM. Therefore, spectral features which are intrinsic to the galaxy at wavelengths shorter than $Ly\alpha$, and which can be completely wiped out by individual $Ly\alpha$ forest systems along a specific line of sight, become visible in the composite spectra. While we regain spectroscopic information by averaging over many different sightlines, we still, however, see the average decrement of the $Ly\alpha$ forest, D_A . In the following section, we describe the spectroscopic features contained in the composite spectrum of Figure 2, which trace the photospheres and winds of massive stars, neutral and ionized gas associated with large-scale outflows, and ionized gas in H II regions where star formation is taking place.

4.1. Stellar Features

The C III $\lambda 1176$, O IV $\lambda 1343$, and S V $\lambda 1501$ stellar photospheric lines discussed in section 3.1 are marked in Figure 2. Also of note (though not marked) is the large number of weak absorption features between 1400 and 1500 \AA . These include blends of Fe V, Si II, Si III, and C III photospheric absorption lines from O and B stars (Bruhweiler, Kondo, & McClusky 1981; de Mello, Leitherer, & Heckman 2000). In addition to photospheric absorption features, the spectra of the most massive hot stars indicate the presence of stellar winds of 2000 - 3000 km s^{-1} due to radiation pressure (Groenewegen, Lamers, & Pauldrach 1989). These wind features appear as broad blue-shifted absorption for weaker winds, or as a P-Cygni type profile if the wind density is high enough (Leitherer, Robert, & Heckman 1995). The most prominent stellar wind features are N V $\lambda\lambda 1238, 1242$, Si IV $\lambda\lambda 1393, 1402$, C IV $\lambda\lambda 1548, 1550$,

and He II $\lambda 1640$. The shape of the N V wind profile, especially the absorption component, is affected by its close proximity to the $Ly\alpha$ region of the spectrum, and is therefore difficult to characterize in detail, though we do see both emission and absorption qualitatively consistent with a P-Cygni type profile. While clear of the large-scale continuum effects of $Ly\alpha$, the Si IV and C IV transitions contain the combination of stellar wind and photospheric absorption, plus a strong interstellar absorption component, which are difficult to disentangle. The stellar wind feature only becomes apparent in Si IV for blue giant and supergiant stars, while, in contrast, the C IV wind feature is strong in main sequence, giant, and supergiant O stars (Walborn & Panek 1984). Consequently, the interstellar, rather than the wind component, seems to dominate the Si IV doublet in the LBG composite spectrum, while the C IV feature exhibits both the blue-shifted broad absorption and redshifted emission associated with stellar winds, in addition to a strong, narrower, interstellar absorption component. The redshifted emission indicates the presence of stars with $M \geq 30M_{\odot}$ (Leitherer, Robert, & Heckman 1995; Pettini et al. 2000). In Figure 3, a Starburst99 model spectrum (Leitherer et al. 1999) is plotted over the zoomed-in C IV $\lambda\lambda 1548, 1550$ region of the LBG composite spectrum for comparison. The model spectrum is for a 300 Myr old episode of continuous star formation (the median stellar population age inferred from the optical/near-IR colors of LBGs, Shapley et al. 2001), and is constructed from a library of HST FOS and STIS observations of massive hot stars in the Magellanic Clouds with a mean metallicity $Z = 0.25Z_{\odot}$ (consistent with the limited information on LBG metallicities). The model and data agree quite well in the emission component of the P-Cygni profile. However, the model overpredicts the strength of the broad wind absorption. This discrepancy may be due to a combination of age and metallicity effects.

The composite LBG spectrum also shows He II $\lambda 1640$ emission which is quite strong compared with observations in local starburst galaxies (Heckman et al. 1998). Narrow He II $\lambda 1640$ emission is seen in galaxy spectra with strong nebular emission. If massive stars are forming in He III regions, He II $\lambda 1640$ can appear as a nebular recombination emission line (from supernovae remnants or superbubbles) (Leitherer, Robert, & Heckman 1995). The He II $\lambda 1640$ emission in the composite LBG spectrum, though, is quite broad, with FWHM $\sim 1500 \text{ km s}^{-1}$. This is visibly broader than the most of the other weak emission lines in the spectrum originating in H II nebular regions, so we favor a stellar wind origin for the He II feature. Broad stellar He II emission is predominantly produced in fast, dense winds from Wolf-Rayet (W-R) stars, which are the evolved descendants of O stars more massive than $M > 20$ - $30M_{\odot}$. Therefore, the strength of the He II emission should provide information about the ratio of W-R to O stars (Schaerer & Vacca 1998).

In order to interpret the He II line, we use Starburst99 population synthesis codes (Leitherer et al. 1999). Model UV spectra of both solar and $0.25 \times$ solar metallicity are produced by Starburst99. The solar metallicity spectrum extends from 1200 - 1800 \AA , which includes the He II line, but the sub-solar metallicity model only extends from 1200 - 1600 \AA . While the current best estimates of LBG metallicities (Pettini et al. 2002, 2001) are closer to $Z = 0.25Z_{\odot}$, we can still use the solar metallicity model spectra to make some interesting inferences. The observed strength of the LBG He II emission line can be matched using a 3 Myr old instantaneous burst model with a

⁴ The precise wavelengths are C III $\lambda 1175.71$, O IV $\lambda 1343.35$, which is a blend of lines at $\lambda = 1342.99$ and $\lambda = 1343.51$, and S V $\lambda 1501.76$

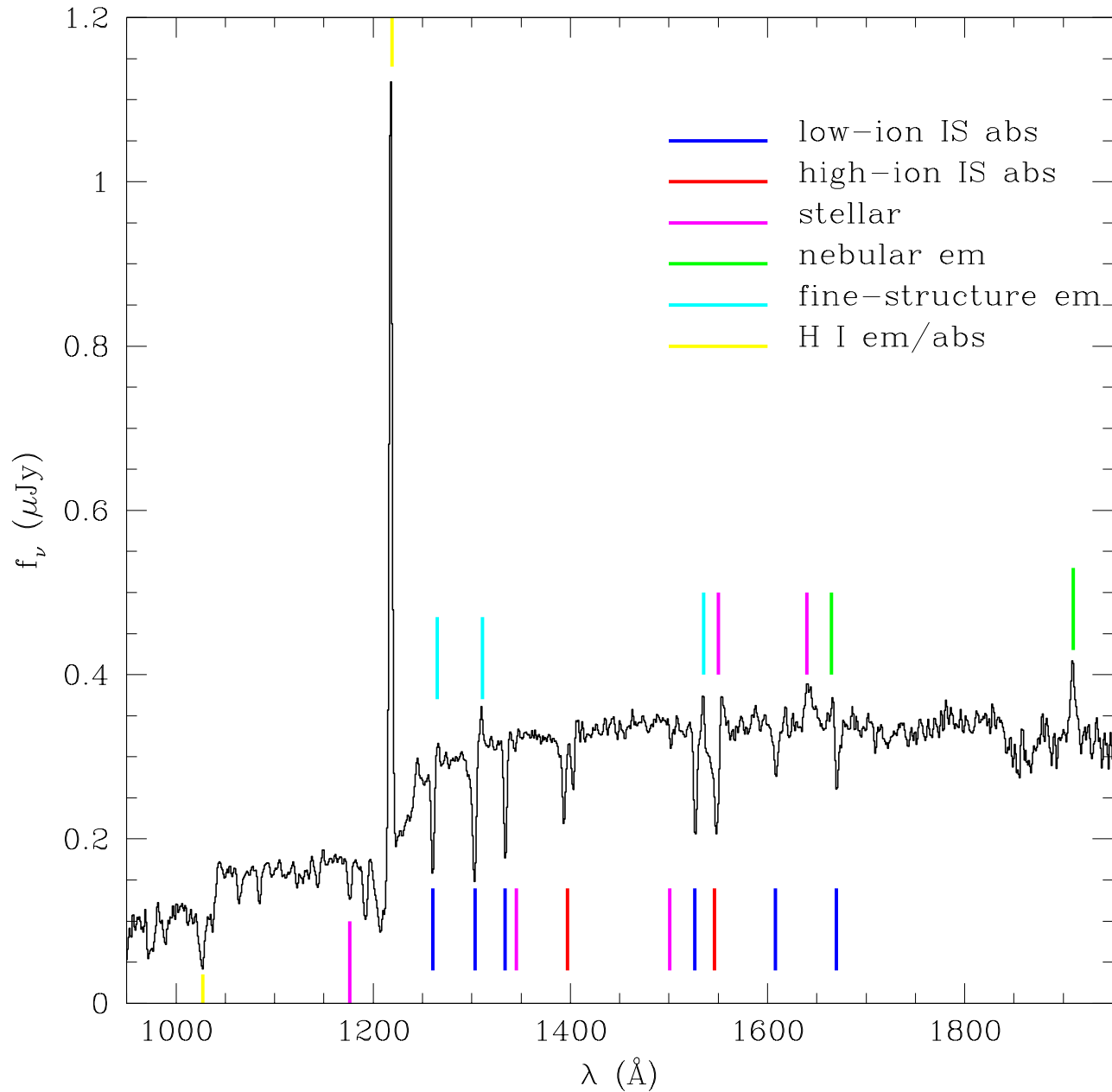


FIG. 2.— A composite rest-frame UV spectrum constructed from 811 individual LBG spectra. Dominated by the emission from massive O and B stars, the overall shape of the UV continuum is modified shortward of $\text{Ly}\alpha$ by a decrement due to inter-galactic HI absorption. Several different sets of UV features are marked: stellar photospheric and wind, interstellar low- and high-ionization absorption, nebular emission from H II regions, Si II* fine-structure emission whose origin is ambiguous, and emission and absorption due to interstellar HI ($\text{Ly}\alpha$ and $\text{Ly}\beta$). There are numerous weak features which are not marked, as well as several features bluewards of $\text{Ly}\alpha$ which only become visible by averaging over many sightlines through the IGM. The composite LBG spectrum is available in electronic form from <http://www.astro.caltech.edu/~aes/lbgspec/>.

standard Salpeter IMF. This is the brief period, following a burst of star formation, when the fractional contribution of Wolf-Rayet stars to the integrated UV luminosity reaches a maximum. Such young burst ages have indeed been derived for Wolf-Rayet galaxies, whose strong optical and UV He II emission lines indicate the presence of numerous high-mass stars and a high W-R/O star ratio (Conti, Leitherer & Vacca 1996; Leitherer et al. 1996). It is not clear which average stellar population is represented by the composite spectrum in Figure 2, but since LBG rest-frame UV/optical SEDs indicate a wide range of properties and ages, and are generally not well-represented by instantaneous burst models (Shapley et al. 2001; Papovich, Dickinson, & Ferguson 2001), it seems extremely unlikely that the 3 Myr old burst model can be representative of the whole population and accordingly we rule out this interpretation.

If we then consider 300 Myr continuous star-formation models (based on the median age derived from SED-fitting), the only way to produce a high enough W-R/O star ratio is to invoke an IMF slope much flatter than the standard Salpeter form of $N(m) \propto m^{-\alpha}$ with $\alpha = 2.35$. Slopes of $\alpha \leq 1$ match the He II strength, but then the C IV P-Cygni emission is overproduced by a factor of ≥ 4 . The discrepancy will be even worse for the sub-solar metallicity models. The ratio of W-R/O stars decreases as a strong function of decreasing metallicity, since the lower-limit on the masses of O stars which evolve into W-R stars moves towards higher masses as the metallicity increases (Maeder 1991; Meynet 1995). Theoretical predictions of W-R line luminosities (Schaerer & Vacca 1998; Leitherer et al. 1999) show that, for a given IMF, 300 Myr continuous star-formation models with $Z = 0.25Z_{\odot}$ have He II $\lambda 1640$ line strengths only half as strong as in the case of solar-metallicity. A more drastic adjustment to the slope of the IMF would be required for the sub-solar metallicity model to match the He II emission strength, which would then lead to an even larger discrepancy for the C IV P-Cygni emission (since, empirically, we measure that the C IV P-Cygni emission does not depend very significantly on metallicity). Clearly, current population synthesis models do not simultaneously reproduce the C IV and He II stellar wind features in LBGs for reasonable choices of star-formation history, age, metallicity, and IMF slope. We will be able to test this discrepancy better with high-quality spectra for individual LBGs whose stellar population ages and star-formation histories we know more accurately than our rough estimate of the stellar population represented by the composite of all the LBGs.

4.2. Outflow-related Features

The large-scale outflow of interstellar material appears to be a generic feature of LBGs, one implied both by the typical LBG star-formation rate per unit area, and also by the fairly ubiquitous observed offset in velocity between Ly α emission and interstellar absorption lines when both sets of lines are seen. Spectral features probing neutral outflowing gas are H I Ly α and Ly β , and neutral and singly ionized metal absorption lines. More highly ionized metal lines probe the ionized phase of the outflow (Heckman et al. 2001b; Pettini et al. 2002). While the interstellar absorption lines in $\sim 70\%$ of individual LBG spectra are strong enough that an absorption redshift can be assigned to at least one low- or high-ionization feature, it is not possible to obtain robust equivalent width measurements for multiple features due to the typical low S/N (and prevalent sky-subtraction residuals). However, in composite spectra containing hundreds

of LBGs, these features are detected with high significance. In this section, we describe the average properties of the spectral features related to the large-scale outflows in LBGs.

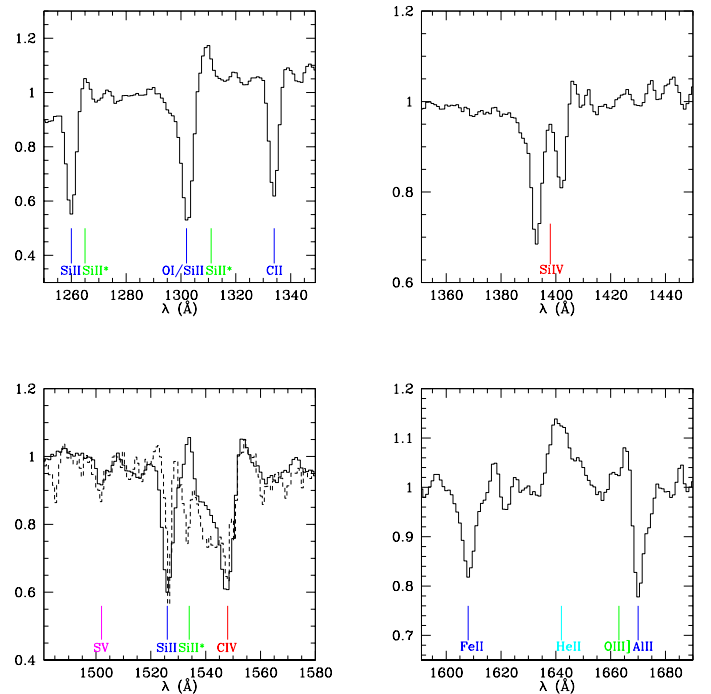


FIG. 3.— Four zoomed-in regions from the composite spectrum of Figure 2. The zoomed-in vertical scale allows a more detailed look at weak nebular emission features such as Si II* $\lambda\lambda 1265, 1309, 1533$, and O III] $\lambda\lambda 1661, 1666$, which are produced in H II regions. The lower left-hand box shows the zoomed-in region near C IV $\lambda\lambda 1548, 1550$. The observed composite spectrum is plotted as a solid line, while the dashed line is a Starburst99 model spectrum for 300 Myr of continuous star-formation with $Z = \frac{1}{4}Z_{\odot}$ (Leitherer et al. 1999, 2001). The model and data agree well for the emission component of the C IV P-Cygni stellar wind line, but the model overpredicts the amount of broad, blue-shifted absorption. This may be due to the lower average metallicity or older age of the LBGs included in the composite spectrum, relative to the model. The lower right-hand box shows the zoomed-in region near the He II $\lambda 1640$ stellar wind line, whose large strength we have trouble reproducing using Starburst99 models with reasonable parameters.

4.2.1. Low-ionization Lines Associated with Neutral Gas

The strongest low-ionization interstellar lines probing outflowing interstellar material are marked in Figure 2, and include Si II $\lambda 1260$, O I+Si II $\lambda 1303$ (a blend at the spectral resolution of our sample), C II $\lambda 1334$, Si II $\lambda 1526$, Fe II $\lambda 1608$, and Al II $\lambda 1670$. While there are additional interstellar absorption lines at wavelengths shorter than Ly α , as well as a host of other, weaker, low-ionization interstellar absorption lines, we confine the analysis in section 5 to these six strongest features redward of Ly α , which we detect at very high significance. The features marked have been well-studied in local starburst galaxies (Gonzalez Delgado et al. 1998; Heckman et al. 1998), as well as in the lensed LBG, MS1512-cB58 (Pettini et al. 2000, 2002). Relative to the stellar, systemic redshift, we measure an average blueshift for the strong low-ionization interstellar features of $\Delta v = -150 \pm 60 \text{ km s}^{-1}$. Using the C II $\lambda 1334$ and Si II $\lambda 1526$ features, which we assume to be the least affected by blends, and assuming an effective spectral resolution of 2.6 \AA for the LBG composite spectrum, we compute the av-

average deconvolved velocity full-width⁵ for the low-ionization interstellar (LIS) lines, $\text{FWHM(LIS)} = 560 \pm 150 \text{ km s}^{-1}$. The largest uncertainty affecting this measurement is the uncertainty of the effective spectral resolution of the composite spectrum, which we conservatively estimate to range between $2 - 3.25 \text{ \AA}$ (roughly $400 - 700 \text{ km s}^{-1}$). The upper bound on the spectral resolution is set by the minimum FWHM value measured for any of the strong interstellar absorption lines. The lower bound of 2 \AA is set by our estimate of the spectral resolution provided by the optimum observing conditions.⁶

We list rest-frame equivalent widths and relative systemic redshifts for the six strongest low-ionization interstellar absorption lines in Table 1. The strength of these features makes them ideal for measuring interstellar absorption redshifts in noisy individual spectra. However, they are not useful for measuring chemical abundances, due to the fact that all of the strong lines are saturated. The saturation of the strong lines is most easily demonstrated by comparing the equivalent widths for two different Si II transitions: Si II $\lambda 1260$ and $\lambda 1526$. On the linear part of the curve of growth, $W \propto Nf\lambda^2$, where N is the column density of the ionic species and λ is the rest-frame wavelength of the transition. According to the relative oscillator strengths and wavelengths of the two Si II transitions, the ratio $W_0(1260)/W_0(1526) > 5$ on the linear part of the curve of growth. We measure $W_0(1260)/W_0(1526) = 0.95$, consistent with a ratio of unity, given the uncertainties, thus demonstrating that the Si II transitions are optically thick. There are weaker features detected in the composite LBG spectrum which probe the linear part of the curve of growth, and which have been used to derive metal abundances in the outflow of MS1512-cB58 (Pettini et al. 2000, 2002). These include S II $\lambda\lambda 1250, 1253, 1259$, Si II $\lambda 1808$, Fe II $\lambda 1144$, Ni II $\lambda 1317, \lambda 1370, \lambda 1703, \lambda 1709, \lambda 1741, \text{ and } \lambda 1751$. Most of these features are detected with only marginal significance in the composite LBG spectrum due to low spectral resolution. An abundance determination also requires an estimate of the H I column density, which is not easily measured from the composite spectrum, due to the way in which it was combined. In this paper, the analysis of the low ions in the outflowing gas is confined to the properties of the strong transitions.

4.2.2. High-ionization Lines Associated with Ionized Gas

In addition to the low-ionization features associated with neutral outflowing gas, we detect high-ionization interstellar features such as Si IV $\lambda\lambda 1393, 1402$, C IV $\lambda\lambda 1548, 1550$, and N V $\lambda\lambda 1238, 1242$. These features predominantly trace gas at $T \gtrsim 10^4 \text{ K}$, which has been ionized by a combination of radiation from massive stars and collisional processes associated with the outflow. We also detect O VI $\lambda\lambda 1032, 1038$ in absorption. If the radiation field is dominated by the spectrum of hot stars, rather than an AGN, O VI is likely to arise in collisionally ionized gas, indicating the presence of an even hotter phase with $T \gtrsim 10^5 \text{ K}$ (Heckman et al. 2001b).

Section 4.1 included a discussion of the stellar winds indicated by the Si IV, C IV, and N V profiles. In this section we consider the properties of the interstellar contributions to the same high-ionization transitions. Again, the proximity of N V to Ly α prevents us from studying this transition in detail,

though we do see evidence for an interstellar absorption component. Also, it is difficult to characterize the properties of the hot phase traced by O VI, due to the fact that the O VI absorption is fairly weak, blended with C II $\lambda 1036$ absorption, and resides in the red wing of the strong Ly β profile. However, we measure $\Delta v = -180 \text{ km s}^{-1}$ for both members of the Si IV transition, which has a doublet ratio of roughly 2:1, indicating that the lines are on the linear part of the curve of growth. We measure $\Delta v = -390 \text{ km s}^{-1}$, for what we isolate as the interstellar component of the C IV absorption, assuming a saturated doublet ratio of 1:1 and therefore a rest-frame centroid of $\lambda = 1549.479 \text{ \AA}$. The measurement of the C IV interstellar velocity is fairly uncertain, due to the combination of P-Cygni emission and broad absorption, possible nebular emission, and interstellar absorption all superposed on one another. The properties of the Si IV and C IV interstellar absorption lines are listed in Table 1.

In light of the complexities associated with the C IV doublet, we emphasize the comparison between the Si IV doublet and the low-ionization lines. The blueshift of the Si IV doublet ($\Delta v = -180 \text{ km s}^{-1}$) agrees quite well with the average blueshift of the strong low-ionization interstellar lines ($\Delta v = -150 \text{ km s}^{-1}$). Furthermore, the average deconvolved velocity full-width for the two members of the Si IV doublet is $\text{FWHM(Si IV)} = 590 \pm 140 \text{ km s}^{-1}$, very similar to the average FWHM for the low-ionization lines. The deconvolved velocities associated with either the Si IV or low-ionization lines are very uncertain due to the uncertainties in spectral resolution. Independent of the resolution of the composite spectrum, however, both the blue-shifts and the un-deconvolved velocity widths of the low and high ionization lines are consistent with each other.

The properties of low and high ionization absorption profiles were compared in the spectrum of the gravitationally lensed LBG, MS1512-cB58, using ~ 10 times higher spectral resolution (Pettini et al. 2002). In the case of cB58, which has much stronger than average low-ionization interstellar absorption lines, saturated Si IV and C IV transitions, and Ly α dominated by a damped absorption profile, absorptions from low-ions and high-ions span the same overall velocity range. Also, the material with the highest optical depth (i.e. where the lines are black) is blueshifted by roughly the same amount for the low ions and the high ions, to within 20 km s^{-1} . One distinction highlighted by Pettini et al. (2002) is that the high-ionization lines show smoother absorption profiles, while the low-ionization profiles break up into a number of discrete components. Composite LBG spectra do not have sufficient spectral resolution to discern qualities such as profile smoothness or clumpiness. However, the overall agreement between low and high ion stages in mean blueshift and velocity FWHM is consistent with the high-resolution results from cB58. In contrast, Wolfe & Prochaska (2000a) find distinct kinematic properties for low and high-ionization transitions associated with damped Ly α absorbers. Specifically, the mean velocities of low and intermediate (Al III) ionization stages differ from those of the high ions, although within each of these two sets of lines there is normally very good internal velocity agreement. Also, in 29 out of 32 cases, the velocity width of the high-ionization absorption exceeds that of the low-ionization absorption. The kinematic

⁵ By deconvolved velocity full-width, FWHM_{int} , we mean the square-root of the difference in quadrature between the observed full-width, FWHM_{obs} and the instrumental resolution, FWHM_{inst} : $\text{FWHM}_{int} = (\text{FWHM}_{obs}^2 - \text{FWHM}_{inst}^2)^{1/2}$

⁶ The spectra were obtained through $1''/4$ slits, which is much larger than the LBG size in typical seeing conditions ($0''.5 - 1''.0$). Under such conditions, the spectral resolution was dictated by the angular sizes of objects falling within slits (i.e. the seeing), rather than by the slit-width.

differences between LBGs and DLAs are another manifestation of the differing characteristics of these two populations of high redshift galaxies, which also exhibit distinct clustering properties (Adelberger et al. 2002a) and metallicities (Pettini 2002). Such differences will eventually help us clarify the true nature of damped Ly α absorption systems.

4.2.3. Ly α

By far the most prominent feature in individual LBG spectra is H I Ly α . The original sources of most Ly α photons are recombinations in H II regions. While the Ly α equivalent width is sensitive to conditions in the H II regions such as temperature, metallicity, star-formation rate, and star-formation history, resonant scattering of Ly α in LBGs by interstellar H I makes the emergent Ly α profile at least as sensitive to the geometry, kinematics, and dust content of the large-scale outflows. When seen in emission, Ly α can be used to measure a redshift. In the composite LBG spectrum shown in Figure 2, we measure a Ly α emission redshift of $\Delta v = +360 \text{ km s}^{-1}$. This relative redshift reflects the fact that a Ly α photon has a much better chance of escaping a galaxy if its last scattering occurs off of an atom which is redshifted with respect to the bulk of the neutral material in the galaxy, imparting a Doppler shift which takes the Ly α photon off resonance. We measure a deconvolved emission full-width of $\text{FWHM}(\text{Ly}\alpha) = 450 \pm 150 \text{ km s}^{-1}$. When seen in absorption, the Ly α feature can be quite broad, with blueshifted absorption extending from zero velocity down to $\Delta v \leq -5000 \text{ km s}^{-1}$. Broad Ly α absorption is therefore not a precise redshift indicator. In spectra with Ly α seen only in absorption, interstellar metal lines can be used to measure the redshift more precisely.

A wide distribution of Ly α profiles is seen in the LBG spectroscopic sample, ranging from damped absorption to emission an order of magnitude stronger than the feature shown in Figure 2 (Steidel et al. 2000). In section 5.3, we will discuss how several LBG spectroscopic properties depend on Ly α equivalent width, and what inferences can be drawn about the physical conditions which determine the emergent Ly α profile. The composite spectrum shown in Figure 2 has a Ly α feature dominated by emission. The total rest-frame equivalent width is $W_0 = 14.3 \text{ \AA}$ which includes both redshifted emission, and much weaker blueshifted absorption. This spectrum is the average of all the LBG spectra in the spectroscopic sample, yet there are selection effects which depend on both apparent \mathcal{R} magnitude, color, and spectroscopic type, which bias the spectrum relative to a true “average” of the total LBG photometric sample. For example, the spectroscopic sample over-represents bright objects relative to faint objects, and the number of objects with Ly α emission relative to those with only Ly α absorption. As discussed in section 5.1, it becomes much more difficult at fainter magnitudes to identify spectroscopically a galaxy with no Ly α emission. Therefore, as the number of spectroscopically unidentified objects increases at fainter magnitudes, so does the ratio of emission to absorption line galaxies with measured redshifts. Accordingly, the Ly α feature in Figure 2 may be biased towards stronger emission than the true average for the total photometric sample. In order to quantify this bias, a more detailed treatment of selection effects is required.

4.3. Emission Lines

One of the benefits of producing a high S/N ratio composite spectrum is that it can reveal weak spectral features

which would have remained undetected in individual spectra. We detect several weak emission lines, some of which we attribute to nebular regions photoionized by radiation from massive stars, and others whose origin is still ambiguous. The weak emission lines in the LBG composite spectra are: Si II* $\lambda 1265$, Si II* $\lambda 1309$, Si II* $\lambda 1533$, O III] $\lambda \lambda 1661, 1666$, and C III] $\lambda \lambda 1907, 1909$. We measure a mean velocity of $\Delta v = 100 \pm 35 \text{ km s}^{-1}$ for the Si II* transitions. The centroids of the fine-structure emission lines may be biased to the red by weak fine-structure absorption lines or neighboring saturated resonance absorption features (Si II $\lambda 1260$, O I+Si II $\lambda 1303$, and Si II $\lambda 1526$) associated with the outflow, which attenuate the blue edges of the fine-structure emission profiles. We measure a velocity of $\Delta v = 0 \text{ km s}^{-1}$ for the O III] $\lambda 1663$ doublet, and a velocity of $\Delta v = 40 \text{ km s}^{-1}$ for the C III] $\lambda 1909$ transition, both of which agree very well with the stellar systemic velocities (section 3.1). O III] $\lambda 1663$ and C III] $\lambda 1909$ are both collisionally excited, semi-forbidden transitions, so there is no absorption from these ions in the large-scale outflow of gas. While the Al II $\lambda 1670$ resonance absorption feature is fairly close to O III], the C III] transition should be clear of any absorption line. There may be a nebular emission component in C IV $\lambda \lambda 1548, 1550$, but it is difficult to isolate nebular C IV emission from the stellar P-Cygni emission. The properties of the emission lines are summarized in Table 2.

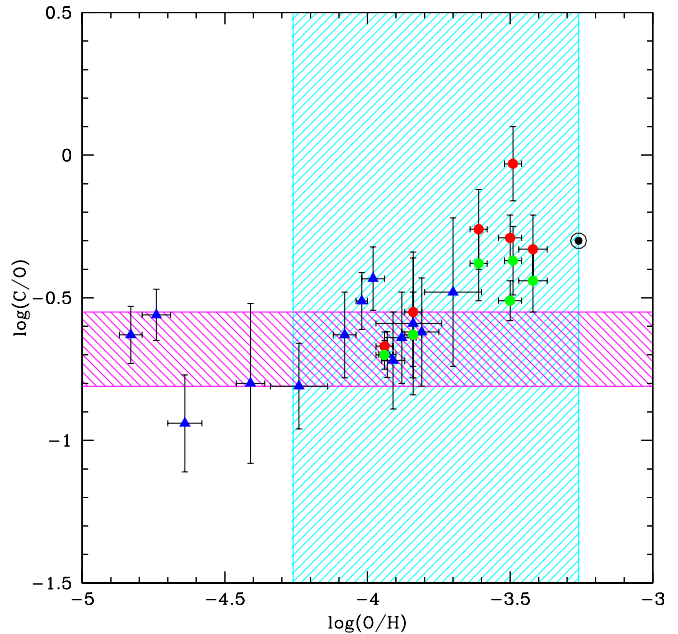


FIG. 4.— $\log(\text{C}/\text{O})$ vs. $\log(\text{O}/\text{H})$ for local H II regions. Blue triangles are data from dwarf irregular galaxies and the Magellanic Clouds (Garnett et al. 1995, 1997; Kobulnicky & Skillman 1998). Spiral galaxy data are shown with circles Garnett et al. (1999). Red symbols assume a shallow ($R_V = 3.1$) Milky Way extinction curve, whereas green symbols indicate a steeper ($R_V = 5.0$) one. The solar abundances (Holweger 2001; Allende Prieto, Lambert, & Asplund 2002) are indicated by the large bulls-eye. The horizontal (magenta) shaded area indicates the $\log(\text{C}/\text{O})$ confidence region derived from the total composite LBG spectrum. The vertical (cyan) shaded area indicates the range of $\log(\text{O}/\text{H})$ implied by the ratio of [O III], [O II], and H β line-strengths in a small sample of bright LBGs (Pettini et al. 2001).

4.3.1. AGN Contribution?

Even though all galaxy spectra flagged as narrow- or broad-lined AGN on an individual basis were removed from the LBG

composite spectra sample, the presence of weak emission lines in the LBG composite spectrum may reveal some average low-level of nuclear activity in LBGs. To address this issue, we examined the emission line ratios in a composite spectrum of 198 LBGs with rest-frame $W_{\text{Ly}\alpha} \geq 20 \text{ \AA}$ in emission (see section 5.3). The nebular emission lines in this composite spectrum are also stronger than those marked in the total LBG spectrum of Figure 2. We compared the emission line ratios in this strong-emission spectrum with those in a composite spectrum of 16 LBGs flagged as narrow-lined AGN on an individual basis (Steidel et al. 2002). The average $\text{Ly}\alpha$ emission equivalent width in this strong-emission (yet not AGN-flagged) subsample is only half as large the emission strength in the narrow-line AGN spectrum. The narrow-line AGN spectrum has line intensity ratios of $\text{C IV}/\text{Ly}\alpha \sim 0.25$, and $\text{C III]/Ly}\alpha \sim 0.125$, which are very similar to the mean ratios of $\text{C IV}/\text{Ly}\alpha = 0.21 \pm 0.09$ and $\text{C III]/Ly}\alpha = 0.10 \pm 0.05$, measured for a sample of four local Seyfert 2 galaxies by Ferland & Osterbrock (1986). In contrast, the non-AGN spectrum has intensity ratios of $\text{C IV}/\text{Ly}\alpha \leq 0.02$ and $\text{C III]/Ly}\alpha = 0.05$. The 2% represents a strict upper limit on the ratio of nebular $\text{C IV}/\text{Ly}\alpha$ (which is probably much smaller), since the total C IV emission represents the sum of nebular emission plus stellar P-Cygni emission. Clearly, the ratios of both C III] and C IV to $\text{Ly}\alpha$ are much smaller in the non-AGN LBG spectrum than in the narrow-line AGN spectrum. Additionally, the ratio of $\text{C III]}/\text{C IV}$ is significantly higher in the non-AGN spectrum than in the AGN spectrum, indicating a softer photoionizing radiation field, more likely dominated by the emission from hot stars rather than non-thermal processes.

4.3.2. C/O Abundance

Ultraviolet spectroscopic observations of H II regions in nearby irregular and spiral galaxies with the *Hubble Space Telescope* (*HST*) have been used to study how the relative abundances of carbon and oxygen (C/O) depend on oxygen abundance (O/H) (Garnett et al. 1995, 1997, 1999; Kobulnicky & Skillman 1998). Ranging in O/H from less than 0.1 to 1.0 times $(\text{O}/\text{H})_{\odot}$, a compilation of these data is shown in figure 4 and demonstrates a clear trend of increasing C/O with increasing O/H (Garnett et al. 1999). For example, in spiral galaxy H II regions, $\log(\text{C}/\text{O}) \simeq -0.7$ at $\log(\text{O}/\text{H}) = -4.0$, and increases to $\log(\text{C}/\text{O}) \simeq -0.2$ at $\log(\text{O}/\text{H}) = -3.4$ ⁷. While the behavior at the smallest metallicities is less clear, due the unexpectedly high C/O ratio in the extremely metal-poor galaxy, I Zwicky 18, the H II regions in other sub-solar metallicity irregular galaxies show the same overall trend as the spiral galaxies (Garnett et al. 1995). Stellar evolution models including stellar winds from massive stars predict that the carbon yield from massive stars increases relative to the oxygen yield, with increasing metallicity (Maeder 1992). These models successfully reproduce both the observed local trend in C/O with O/H, and also C/O abundance gradients in Galactic stars and H II regions (e.g. Carigi 2000). While the rise of C/O with O/H in local star-forming regions is mainly due to yields from massive stars, there is also the fact that oxygen is primarily synthesized in stars with $M > 10M_{\odot}$, whereas carbon is produced in both high and intermediate mass ($2-8M_{\odot}$), delaying in time the ejection of some fraction of carbon into the ISM, relative to oxygen. In relatively young galaxies at high redshift, the ob-

served C/O ratio may thus also reflect the average time since the onset of star-formation. In such circumstances, younger stellar populations may be dominated by the chemical yields from the most massive stars, whereas after a few 100 Myr since the onset of star formation, an increased C/O ratio reflects the fact that intermediate-mass stars have had a chance to release their carbon into the ISM.

Since we detect both $\text{C III] } \lambda 1909$ and $\text{O III] } \lambda 1663$ in the LBG composite spectrum shown in Figure 2, we follow the analysis of Garnett et al. (1995), assuming that the electron densities in these H II regions are well below the critical limit for the C III] and O III] transitions. In the low-density limit, we can express the relative abundances of C^{+2} and O^{+2} as:

$$\frac{\text{C}^{+2}}{\text{O}^{+2}} = \frac{1}{9} \times \frac{\Omega_{\text{OIII]}}(^3\text{P}, ^5\text{S}_2)}{\Omega_{\text{CIII]}}(^1\text{S}, ^3\text{P})} \times \frac{\lambda_{\text{CIII]1909}}}{\lambda_{\text{OIII]1663}} \times e^{-11054/T} \times \frac{I(\text{CIII]}\lambda 1909)}{I(\text{OIII]}\lambda 1663)} \quad (2)$$

In this expression $\Omega_{\text{OIII]}}(^3\text{P}, ^5\text{S}_2)$ and $\Omega_{\text{CIII]}}(^1\text{S}, ^3\text{P})$ are the multiplet collision strengths for the $\text{O III] } \lambda 1663$ and $\text{C III] } \lambda 1909$ doublets, which have a weak temperature dependence (see Garnett et al. 1995 for specific collision-strength values); the prefactor of $\frac{1}{9}$ represents a combination of statistical weights; $\lambda_{\text{CIII]1909}}$ and $\lambda_{\text{OIII]1663}}$ are the effective wavelengths of the C III] and O III] doublets; T is the H II region electron temperature; and $I(\text{CIII]}\lambda 1909)$ and $I(\text{OIII]}\lambda 1663)$ are the line intensities. To compute $I(\text{OIII]}\lambda 1663)$ we integrate the flux from both members of the resolved $\text{O III] } \lambda 1663$ doublet (the C III] doublet is unresolved). Strictly speaking, $\text{C}/\text{O} = \text{C}^{+2}/\text{O}^{+2} \times \text{ICF}$, where ICF is an ionization correction factor which takes into account the fact that while C III] and O III] are similar ionization states, C^{+2} has a slightly lower ionization potential than O^{+2} . In practice, Garnett et al. (1995) find ICF only ranges between 1.06–1.33, and so, for lack of any detailed information, we make the approximation $\text{ICF} = 1$ and $\text{C}/\text{O} \simeq \text{C}^{+2}/\text{O}^{+2}$. Based on the measured ratio of C III] and O III] line strengths in the total composite LBG spectrum, we measure $\log(\text{C}/\text{O}) = -0.68 \pm 0.13$. This confidence interval is marked by the horizontal magenta shaded region in Figure 4. The quoted uncertainty corresponds to a temperature range $T = 10000-20000 \text{ K}$, but does not include the uncertainty in the determination of the continuum level, which may amount to an additional error of about a factor of two in the determination of C/O. We measure a very similar value of $\log(\text{C}/\text{O}) = -0.74 \pm 0.14$ in the LBG composite spectrum constructed from the sub-sample which includes only strong emission-line galaxies (see sections 4.3.1, 5.3). Similar C/O ratios are found by Garnett et al. (1999) for galaxies with $\text{O}/\text{H} \sim 0.2 \times (\text{O}/\text{H})_{\odot}$. There are large uncertainties associated with the LBG C/O measurements. However, we note that the corresponding O/H values are consistent with – if towards the low-end of the confidence interval of – the O/H metallicity determinations for LBGs based on the ratio of rest-frame optical nebular $[\text{O II}]$, $[\text{O III}]$, and $\text{H}\beta$ emission lines ($\sim 0.1-1 \times (\text{O}/\text{H})_{\odot}$) (Pettini et al. 2001).⁸ The range in $\log(\text{O}/\text{H})$ deduced by Pettini et al. (2001) is marked by the vertical cyan shaded region in Figure 4. In view of the large uncertainties associated with both C/O and O/H determinations in LBGs, we do not interpret these results any further, except to point out that the comparison of C and O emission strengths will be an interesting diagnostic of

⁷ The solar oxygen abundance is $\log(\text{O}/\text{H})_{\odot} = -3.26$ (Holweger 2001)

⁸ The galaxies with rest-frame optical spectroscopic observations were drawn from the bright end of the LBG UV luminosity function. It is not clear how this selection criterion limits the range of metallicities probed, relative to the abundance range in the LBG sample as a whole.

chemical evolution and stellar populations at high-redshift in future, higher-quality data.

4.3.3. Si II* Lines

In addition to C III] and O III], which have been studied in local star-forming regions, we also detect lines at which we identify as Si II* fine-structure emission lines. Unfortunately, our spectral resolution is too coarse to determine if we detect C II* $\lambda 1335$ Å emission as well (the C II $\lambda 1334$ resonance absorption line from outflowing neutral gas swamps any signal at that wavelength). A literature search of local ultraviolet observations reveals very few references to Si II* fine-structure emission lines. The *International Ultraviolet Explorer (IUE)* atlas of star-forming galaxies compiled by Kinney et al. (1993) contains a census of ultraviolet emission lines associated with nebular objects such as H II regions, planetary nebulae, and supernova remnants, but does not include the Si II* features. The spectral resolution of IUE is ~ 1000 km s⁻¹, coarser than the resolution of the LBG composite spectra. When the LBG composite spectra are smoothed to the resolution of the IUE data, the Si II* lines are still visible at 5% to 10% above the continuum level. Presumably, the individual IUE spectra contained in the Kinney et al. (1993) atlas are of insufficient S/N to see these features. However, the Si II* features are also not detected in composite starburst spectra containing 20 individual galaxy spectra drawn from the IUE atlas, each of which has continuum S/N of at least 10 (Heckman et al. 1998).

The Einstein A coefficients associated with the Si II* transitions range from $10^8 - 10^9$ s⁻¹, more than six orders of magnitude larger than the A-values for the semi-forbidden O III] and C III] transitions. Only in very high-density environments ($N_e = 10^9 - 10^{13}$ cm⁻³) are the Si II excited level populations determined by collisional excitations and de-excitations (Keenan et al. 1992). In H II regions, where the electron densities are typically $N_e = 10^2 - 10^3$ cm⁻³, collisions are therefore not the dominant mechanism governing the Si II level populations. Also, when $T \sim 10^4$ K and Si II and Si III have comparable abundances (as appropriate here), it can be shown that the recombination rate of Si III into the excited Si II levels is of the same order as the Si II collisional excitation rates (Shull & van Steenberg 1982). In order to understand the origin of the Si II* emission lines in a more systematic way, we modeled all observed LBG nebular emission lines using the CLOUDY96 software package (Ferland et al 1998). The observational constraints are the average rest-frame optical strengths of [O III], [O II], and H β (Pettini et al. 2001), as well as the rest-frame UV O III] and C III] strengths (section 4.3.2). We found that *any* model which provides a satisfactory fit to the O, C, and H β line ratios simultaneously predicts Si II* emission line strengths which are more than an order of magnitude weaker than observed. This result seems to exclude an origin in photoionized H II regions for the Si II* emission lines.

An alternative explanation for these lines is that they are produced in the large-scale outflows in LBGs. UV photons with $\lambda = 1260, 1304, 1526$ are absorbed by ground state Si II in the outflowing neutral gas, as indicated by the saturated Si II resonance absorption transitions. Each photon absorbed in a resonance or fine-structure transition is re-emitted in a transition either to the ground state or the excited ground state, with the relative probabilities determined by the Einstein A-coefficients for the different transitions. In the absence of dust extinction, and if the slit used to observe the galaxy/outflow

system is as large as the region emitting in Si II and Si II*, the sum of the resonant and fine-structure emission equivalent widths should be equal in strength to the absorption from the same transitions. This is clearly not the case, in that the Si II * $\lambda 1265, 1309, 1533$ fine-structure emission lines are an order of magnitude weaker than the Si II $\lambda 1260, 1304, 1526$ resonant absorption lines. We don't even detect any resonant Si II emission, as saturated blue-shifted Si II absorption dominates over emission at $\Delta v = +100$ km s⁻¹, the mean velocity of the Si II* emission lines. The dominance of resonant absorption over fine-structure emission may be due to dust attenuation of Si II photons during resonant scattering. It also may indicate that the slit used in LBG spectroscopic observations only subtends a small fraction of the Si II* emitting region. One problem with interpreting the Si II* emission lines as being produced in the outflowing gas is their kinematic properties. The outflow is optically thin to Si II* (negligible absorption is detected in these transitions), so we expect Si II* emission lines produced in outflowing gas to probe the full range of approaching and receding velocities (≥ 1000 km s⁻¹). In fact, the Si II* lines are barely resolved in the composite spectrum, with FWHM ≤ 500 km s⁻¹. While Si II* emission may be biased towards positive velocities by blue-shifted fine-structure, or even broad resonance, absorption, we expect that it should be at least as broad as the Ly α emission, which is attenuated on the blue edge by much stronger absorption over a wider range of velocities. However, the Si II* lines are narrower than the Ly α emission line, which extends to much more redshifted velocities. In summary, both the outflow and H II region models of the Si II* features fail to explain all of the observed properties of the emission lines, whose true nature remains to be determined.

5. LBG SPECTROSCOPIC TRENDS

We have characterized the basic features of the composite spectrum formed from the $z \sim 3$ LBG spectroscopic sample. We are now ready to examine how these spectroscopic features vary across the sample as functions of different galaxy parameters. Some of the parameters which can be measured for individual galaxies are: redshift, z ; rest-frame UV apparent magnitude, \mathcal{R} ; rest-frame UV color corrected for IGM absorption, $(G-R)_0$, which can be parameterized in terms of a reddening, $E(B-V)$, given an assumed form for the intrinsic spectrum; Ly α rest-frame equivalent width, $W_{Ly\alpha}$; and interstellar kinematics, Δv_{em-abs} . Our spectroscopic sample is large enough that we can divide the total sample into several subgroups based on each of the above parameters, and still create a high S/N composite spectrum for each subgroup. Individual spectra are not of sufficient S/N to be able to reliably measure low- and high-ionization interstellar absorption equivalent widths, W_{LIS} and W_{HIS} . Therefore, we do not bin the sample according to interstellar absorption line strength, but we can measure the interstellar absorption strengths with high significance in all of the composite spectra.

5.1. Selection Effects

Before considering LBG spectroscopic trends, we must isolate which parameters are sensitive to the variance in the underlying galaxy population and which are more sensitive to our photometric and spectroscopic selection criteria. To illustrate the importance of selection effects, we consider how our photometric and spectroscopic biases limit the range of galaxy pa-

parameter space which can be sampled as a function of z and \mathcal{R} magnitude.

First, we examine biases resulting from the LBG photometric selection criteria. One of the LBG color criteria is $G-R \leq 1.2$, which affects the range of intrinsic UV colors selected with the LBG technique as a function of redshift. The reason for this effect is that absorption by HI in the IGM attenuates the flux in the G -band for galaxies with $z \geq 2.4$. The average amount of attenuation is an increasing function of redshift, ranging from $\Delta G = 0$ magnitudes at $z = 2.4$ to $\Delta G = 0.2$ magnitudes at $z = 3.0$, to as much as $\Delta G = 0.5$ magnitudes at $z = 3.4$. Since LBGs are photometrically pre-selected on the basis of observed $G-R$ color, which includes the effect of IGM absorption, the range of intrinsic colors which can be included in the LBG sample is a strong function of redshift. As discussed in section 5.4, the rest-frame UV colors of continuously star-forming galaxies are largely determined by the amount of reddening affecting the stellar continuum, so the intrinsic UV color, $(G-R)_0$ can also be parameterized in terms of $E(B-V)$, once a form of the attenuation curve is assumed (Calzetti 1997; Calzetti et al. 2000). In subsequent discussion, we use $E(B-V)$ to represent both intrinsic UV color and the amount of dust extinction, since there is almost a one-to-one correspondence between the two parameters. Figure 5 shows $E(B-V)$ vs. z for the LBG spectroscopic sample, demonstrating the strong apparent correlation of UV color with redshift, induced by our photometric selection effects.

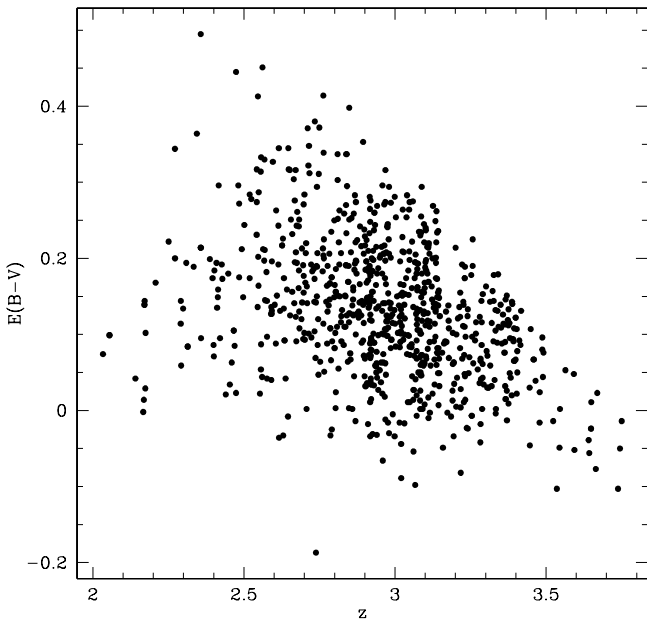


FIG. 5.— The distribution of $E(B-V)$ values as a function of z . Due to the way in which LBGs are color-selected to have *observed* $G-R$ colors which lie within a specific range, the increased IGM absorption affecting the G -band flux as a function of z limits the range of *intrinsic* colors of LBGs (parameterized by $E(B-V)$) at higher z .

There are also important photometric selection effects associated with apparent \mathcal{R} magnitude. Due to the nature of LBG color criteria, and the fact the U_n images have finite depth, the dynamic range in $G-R$ color is limited on average to bluer colors at fainter \mathcal{R} magnitudes. Accordingly, there is a weak apparent correlation between \mathcal{R} and $E(B-V)$, in the sense that fainter LBGs are bluer on average. However, Adelberger

(2002b) demonstrates that, once selection effects are accounted for, \mathcal{R} and $E(B-V)$ are consistent with being independently distributed. The biases against UV color as a function of z and \mathcal{R} magnitude result from the LBG photometric selection criteria and uncertainties, and have been discussed extensively and quantified for the purpose of constructing the LBG rest-frame UV luminosity function (Steidel et al. 1999; Adelberger & Steidel 2000; Adelberger 2002b).

There are two additional spectroscopic sources of incompleteness which affect the sample under consideration. First, not all galaxies in the photometric sample were assigned to slit-masks and observed spectroscopically. This incompleteness is primarily a function of \mathcal{R} magnitude, i.e. a larger fraction of bright galaxies in the photometric sample were observed spectroscopically, relative to the fraction of faint galaxies. The distribution of $G-R$ colors of spectroscopically observed galaxies is relatively unbiased with respect to the photometric sample. Second, not all galaxies observed spectroscopically had successfully measured redshifts. This type of incompleteness also depends on \mathcal{R} magnitude, but the subtlety lies in the fact that galaxies with different spectroscopic types (i.e. those with and without Ly α emission) have different spectroscopic success rates as a function of \mathcal{R} magnitude. Figure 6 shows the spectroscopic incompleteness as a function of magnitude, and Figure 7 shows the incompleteness as a function of both magnitude and spectral type.

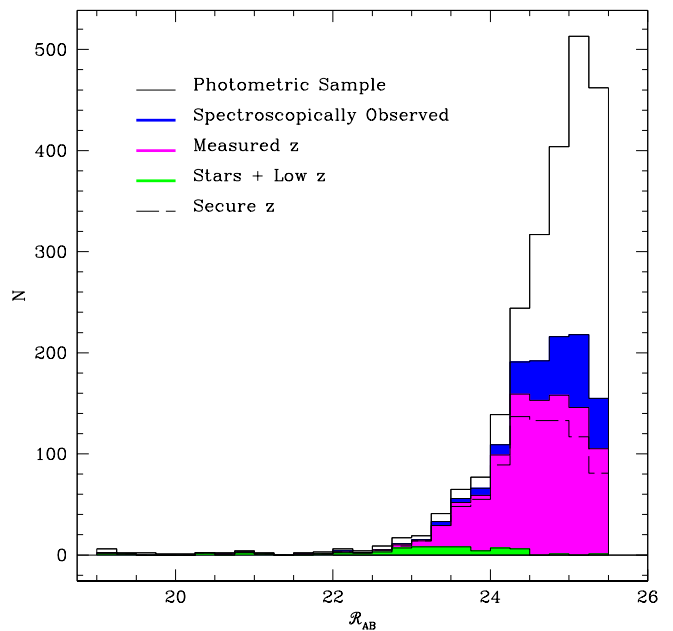


FIG. 6.— Photometric and Spectroscopic incompleteness of the LBG sample as a function of \mathcal{R} magnitude. The empty histogram represents galaxies photometrically selected by their colors to be at $z \sim 3$. The blue histogram consists of galaxies from the photometric sample which were observed spectroscopically. The pink histogram indicates spectroscopically observed objects for which a redshift was successfully measured. The green histogram shows the small fraction of spectroscopically confirmed objects ($\sim 4\%$) which turn out to be stars or low- z galaxies. The dashed histogram shows the subset of spectroscopically confirmed objects which have secure redshifts confirmed by at least two independent members of our group. Non-AGN objects in this secure- z sample with $z > 2$ were included in composite spectra.

There are three subgroups identified in Figure 7: spectra for which the redshift was measured with Ly α emission (some of which also have interstellar absorption redshifts, but which

have at least one identifiable emission line); spectra for which the redshift was only measured with interstellar absorption lines; spectra for which no redshift was measured. Not surprisingly, the fraction of galaxies with spectroscopic failures increases from $\sim 10\%$ at $\mathcal{R} = 24$ to $> 30\%$ at $\mathcal{R} = 25 - 25.5$. The fraction of spectroscopic successes for which the redshift was measured from features including Ly α emission increases from $\sim 60\%$ at $\mathcal{R} = 24$ to $\sim 75\%$ at $\mathcal{R} = 25 - 25.5$. Simultaneously, the fraction of successes for which the redshift was measured only from absorption lines decreases from $\sim 40\%$ at $\mathcal{R} = 24$ down to $\sim 25\%$ at $\mathcal{R} = 25 - 25.5$. These percentages reflect the somewhat obvious fact that it is easier to measure a redshift from an emission line than from an absorption line at fainter magnitudes. As a result, the observed fractions of spectroscopically confirmed objects with and without emission lines in the faintest magnitude bin of Figure 7 do not represent the true underlying fractions, in the sense that emission line objects are overrepresented. We can try to draw inferences about the underlying proportion of emission and absorption objects from the fraction of objects without measured spectroscopic redshifts. The simplest possible assumption is that these galaxies must have Ly α emission fluxes below some limiting value as a function of magnitude. This limiting Ly α flux depends on other factors in addition to \mathcal{R} magnitude, most notably time-dependent observing conditions such as sky transparency and seeing. It is difficult to quantify these effects exactly, so we use the conservative assumption that the galaxies without redshifts have $W_{\text{Ly}\alpha} < 0$, i.e. no Ly α emission, and that if redshifts had been measured for these galaxies they would have only been measured from interstellar absorption lines. If the fraction of galaxies with no redshifts is added to the fraction of galaxies with only interstellar absorption redshifts, we see that the implied true proportion of emission and absorption objects remains roughly constant and equal as a function of magnitude (pink dots in Figure 7), in contrast to the observed proportion (black dots in Figure 7). This exercise gives a rough indication of the degree to which objects with Ly α emission lines are overrepresented relative to absorption-line-only objects within the spectroscopic sample as a function of magnitude.

The photometric and spectroscopic biases presented above affect determinations of both the total LBG spectrum and of the ways in which spectroscopic properties depend on galaxy parameters. Luminosity and redshift are especially prone to these selection effects. Therefore, the discussion of LBG spectroscopic trends is limited to the parameters $W_{\text{Ly}\alpha}$, $E(B-V)$, and $\Delta v_{\text{em-abs}}$. There are highly significant patterns in the spectroscopic properties of LBGs as functions of these parameters. With simple arguments, we show why the strong dependences in the spectroscopic parameters reflect the physical conditions in LBGs, and not the nature of our selection effects.

5.2. Uncertainties

In order to assess the significance of the spectroscopic trends in the sample, it is necessary to assign error bars to the spectroscopic measurements from each composite spectrum. The uncertainty on an equivalent width measurement from a composite spectrum includes not only the finite S/N of the composite spectrum, but also the range of equivalent widths in the sample of galaxies used to construct the composite. While Ly α equivalent widths were measured for almost all of the individual galaxies in the spectroscopic sample, only a subset of the strong interstellar absorption lines was detectable in typical in-

dividual spectra. In fact, in 231 cases Ly α emission was the only spectroscopic feature identified. Additionally, the Si II*, C III], and O III] nebular emission lines are far too weak to be measured in individual spectra.

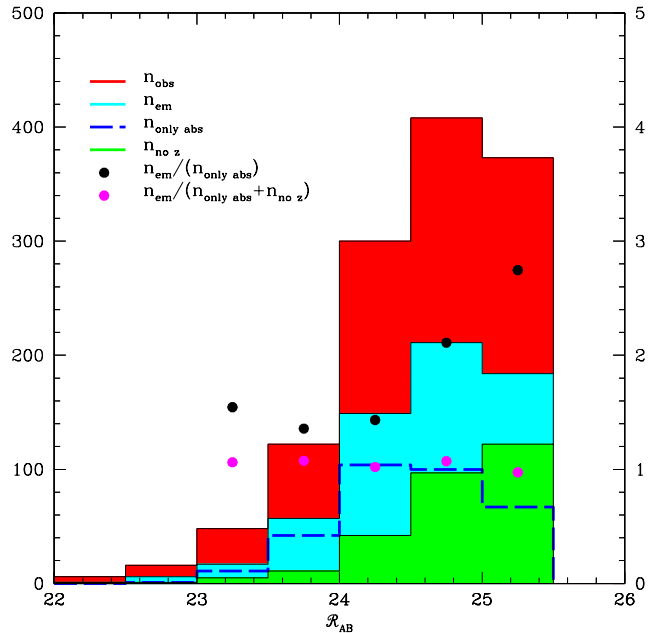


FIG. 7.— Photometric and Spectroscopic incompleteness of the LBG sample as a function of \mathcal{R} magnitude and spectroscopic type. The red histogram shows the number of galaxies observed spectroscopically. The cyan histogram shows the number of galaxies with redshifts measured from features which include Ly α emission. The blue dashed histogram shows the number of objects with no detectable Ly α emission and redshifts measured only from interstellar absorption lines. The green histogram shows the number of objects for which no redshift was successfully measured. The black dots indicate the ratio of galaxies with Ly α emission to those with only absorption line redshifts, which increases steeply as a function of \mathcal{R} magnitude. Based on the assumption that the unidentified objects in the green histogram are $z \sim 3$ galaxies that have $W_{\text{Ly}\alpha} < 0$ and spectra with insufficient S/N to identify absorption features, we see that the ratio of objects with Ly α emission to those with only absorption features remains roughly constant as a function of magnitude (pink dots).

Given that most of the spectroscopic features analyzed in the composites could not be measured reliably in individual spectra, we estimated the sample variance for these features using bootstrap techniques, as follows. For each composite spectrum, we generated 500 fake composite spectra, each one constructed from a sample of galaxies drawn with replacement from the sample used for the real composite spectrum ($\sim 37\%$ of the sample is replaced with duplicates). Using a measurement technique identical to the analysis applied to the real composite spectrum, we continuum normalized each fake composite spectrum, and measured the equivalent widths of Ly α , the six strongest low-ionization interstellar absorption lines, the Si IV and C IV high-ionization interstellar absorption lines, and the weak nebular emission lines. To take into account the noise in each fake composite spectrum, each fake equivalent width measurement was perturbed by an amount drawn from a Gaussian distribution with standard deviation $\sigma = \frac{\sqrt{n}}{S/N}$, where n is the number of pixels over which the equivalent width was measured, and S/N is the signal-to-noise ratio of the real composite spectrum, measured in a relatively featureless portion of the continuum. For the strong interstellar absorption lines and weak emission lines, the contributions to the uncertainty from sample variance and finite S/N were roughly comparable,

while in the case of $\text{Ly}\alpha$, sample variance dominated the uncertainty estimate. The total uncertainty for each real equivalent width measurement was then equal to the standard deviation of the distribution of 500 perturbed fake equivalent width measurements (which were distributed around the actual measured value with no systematic offset). The uncertainties for all quantities measured from composite spectra were derived with the above technique. Bootstrap techniques can also be used to estimate the uncertainty in the mean continuum properties such as $E(B-V)$ and \mathcal{R} magnitude, of each composite sample.⁹

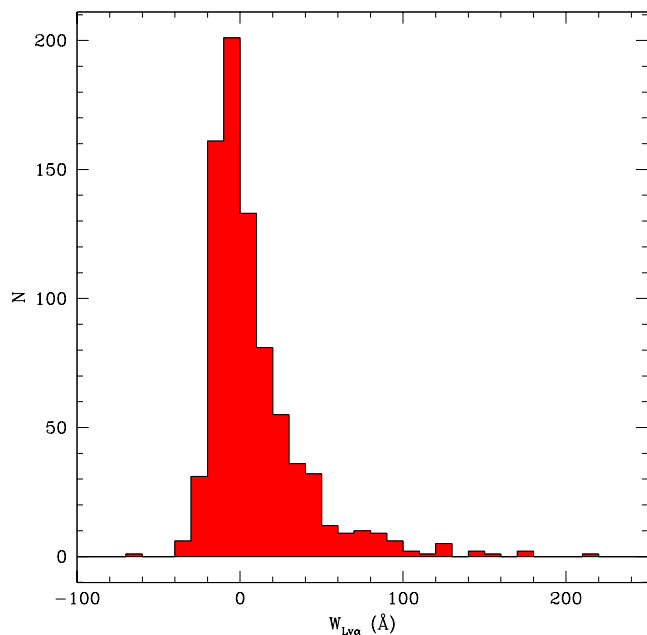


FIG. 8.— The distribution of $\text{Ly}\alpha$ equivalent widths for the LBG spectroscopic sample. This sample contains a broad range of equivalent widths with a median of ~ 0 Å. Only 25% of the sample has rest-frame $W_{\text{Ly}\alpha} \geq 20$ Å, large enough to be selected by narrow band excess techniques, given the depth of current surveys. There is a correlation between $\text{Ly}\alpha$ emission equivalent width and \mathcal{R} magnitude among sources with $W_{\text{Ly}\alpha} \geq 20$ Å, such that fainter galaxies have larger $W_{\text{Ly}\alpha}$.

5.3. $\text{Ly}\alpha$ Dependences

One of the most striking characteristics of the LBG spectroscopic sample is the broad distribution of $\text{Ly}\alpha$ strengths and profile-types, ranging from pure damped absorption, to emission plus absorption, to pure strong emission. There is a large body of theoretical and observational work concerning the physical processes which determine the emergent $\text{Ly}\alpha$ profile in local and high-redshift star-forming galaxies. In local star-forming galaxies, early observations indicated $\text{Ly}\alpha$ emission equivalent widths much smaller than expected from recombination theory, given the star-formation rates inferred from optical Balmer emission lines (Meier & Terlevich 1981; Hartmann, Huchra & Geller 1984; Hartmann et al. 1988). Additionally, these observations offered evidence for a correlation between $\text{Ly}\alpha/\text{H}\beta$ and metallicity (measured from the nebular oxygen abundance, O/H), in the sense that galaxies with lower $\text{Ly}\alpha/\text{H}\beta$ also had higher O/H (Hartmann et al. 1988; Charlot & Fall 1993). The observations were first explained with the

presence of interstellar dust in a uniform medium, which preferentially destroys $\text{Ly}\alpha$ photons relative to non-resonant UV continuum photons, due to the increased path-length traversed by the resonantly scattered $\text{Ly}\alpha$ photons. In addition to affecting $\text{Ly}\alpha$ photons produced by recombinations in H II regions, dust extinction can also attenuate stellar continuum photons in the immediate vicinity of $\text{Ly}\alpha$, which are also resonantly scattered (Charlot & Fall 1993; Chen & Neufeld 1994). The combination of resonant scattering and dust attenuation was thought to significantly reduce the emergent $\text{Ly}\alpha$ emission.

The models of a uniform scattering medium clearly oversimplify the structure of the ISM in star-forming galaxies. There are other factors which introduce complexity into the description of $\text{Ly}\alpha$ radiative transfer, including the geometry and kinematics of the ISM. As described by Neufeld (1991) and Charlot & Fall (1993), the relative geometries of interstellar H I and H II regions significantly affect the transfer of resonantly scattered photons, but in ways which can either suppress or enhance the $\text{Ly}\alpha$ line relative to the continuum. The importance of the geometry of the neutral phase of the ISM is emphasized by the observational results of Giavalisco, Koratkar, & Calzetti (1996a). A lack of correlation between the equivalent width of $\text{Ly}\alpha$ and the UV continuum slope, β (a measure of continuum extinction), is interpreted as evidence for the decoupling of the reddening of line and continuum photons. This decoupling can occur if the neutral ISM (where the dust resides) is inhomogeneous. Due to resonant scattering, for example, $\text{Ly}\alpha$ photons can propagate into paths with less than average gas and dust and escape, whereas the continuum photons reflect the average dust obscuration along the line of sight. The kinematics of the neutral ISM can also affect the emergent $\text{Ly}\alpha$ profile. Inspired by such examples as the metal-poor local starburst I Zwicky 18, which has $\text{Ly}\alpha$ only in absorption (Kunth et al. 1994), and the dustier and more metal-rich Haro 2 which shows a redshifted P-Cygni $\text{Ly}\alpha$ emission feature (Lequeux et al. 1995), Kunth et al. (1998) survey a small sample of local starburst galaxies in the UV, and find that the objects with $\text{Ly}\alpha$ only in absorption also have interstellar absorption lines (O I $\lambda 1302$ and Si II $\lambda 1304$) which are at rest with respect to the H II regions, whereas galaxies with $\text{Ly}\alpha$ emission exhibit asymmetric, P-Cygni $\text{Ly}\alpha$ profiles, with redshifted $\text{Ly}\alpha$ emission, and blueshifted interstellar absorption lines. These observations support a picture in which $\text{Ly}\alpha$ photons mainly escape when they are produced by – or scatter off of – material which is offset in velocity from the bulk of the scattering neutral medium. If the neutral ISM is static with respect to the sources of $\text{Ly}\alpha$ photons, then the covering factor of the neutral gas becomes important (Kunth et al. 1998). Using such observational evidence, Tenorio-Tagle et al. (1999) have developed a detailed model for the way in which outflow kinematics determine the emergent $\text{Ly}\alpha$ profile in starburst galaxies.

At high redshift, a representative subsample of LBG $\text{Ly}\alpha$ equivalent widths (Steidel et al. 2000) show that only ~ 20 –25% of LBGs at $z \sim 3$ at a given UV luminosity have $\text{Ly}\alpha$ emission lines strong enough to be flagged as narrow-band excess objects, given typical high-redshift $\text{Ly}\alpha$ emission line search sensitivities (Cowie & Hu 1998; Hu, Cowie, & McMahon 1998). As discussed below, LBGs with such strong emission have certain properties which make them distinct from the

⁹ Of course, it is also possible to estimate the uncertainty in the mean, $\langle x \rangle$, as $\sigma_{\langle x \rangle} = \frac{\sigma_x}{\sqrt{N_x}}$, where σ_x is the standard deviation of the distribution of x , and N_x is the number galaxies in the sample from which x was measured. This technique yields roughly the same uncertainty in $E(B-V)$ and \mathcal{R} magnitude for each composite sample as the value estimated from the bootstrap method.

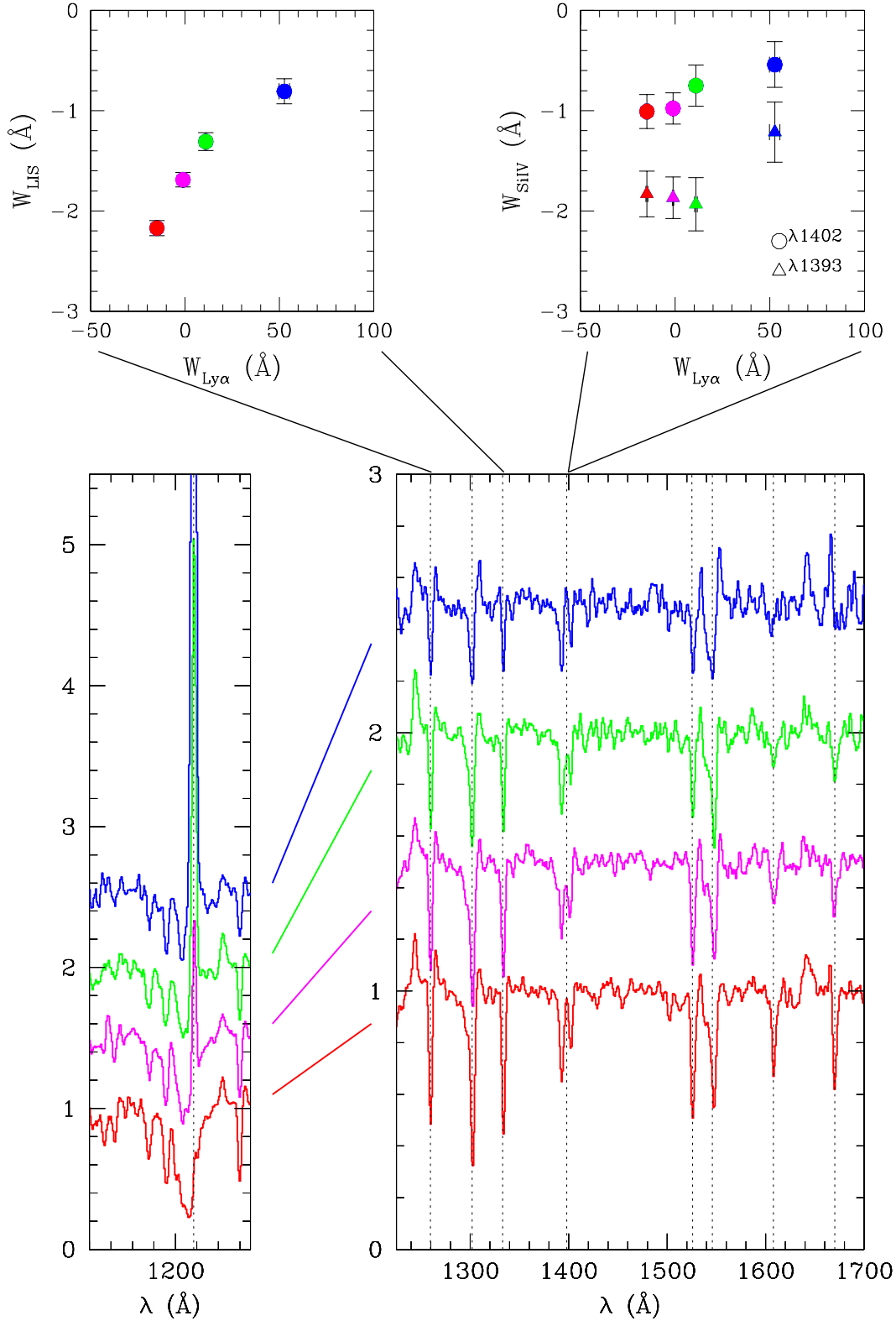


FIG. 9.— Bottom: A sequence of 4 continuum-normalized composite spectra, constructed from the 4 quartiles of LBG spectroscopic sample grouped according to Ly α equivalent width. The spectra have been offset by regular vertical intervals for easier viewing, in order of increasing $W_{\text{Ly}\alpha}$. The lower left-hand panel zooms in on the region near Ly α , while the right-hand panel focuses on the region redwards of Ly α , where the strongest features are blue-shifted low-ionization and high-ionization interstellar absorption features associated with large-scale outflows of interstellar material. Top: The behavior of low- and high-ionization interstellar absorption lines as a function of Ly α equivalent width. These plots confirm quantitatively what the bottom panels indicate visually: the average low-ionization absorption equivalent width, W_{LIS} , decreases dramatically as $W_{\text{Ly}\alpha}$ varies from strong absorption to strong emission, while the high-ionization Si IV absorption equivalent width, W_{SiIV} , remains roughly constant (except in the quartile of the sample with strong Ly α emission, in which W_{HIS} is slightly weaker).

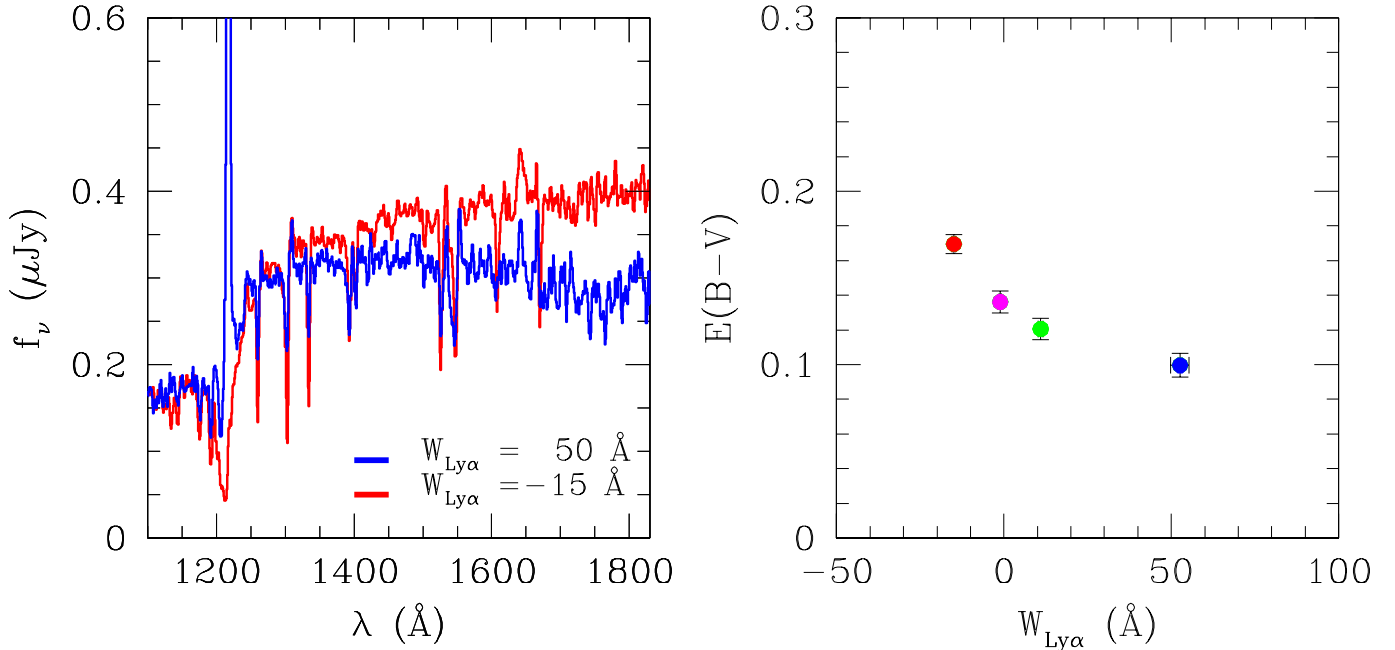


FIG. 10.— The dependence of UV continuum shape on Ly α equivalent width. (left) Plotted in blue, the composite spectrum of the quartile of galaxies with the strongest Ly α emission and the weakest low-ionization interstellar absorption lines is also significantly bluer in spectral slope than the composite spectrum of the quartile of galaxies with the strongest Ly α absorption and strongest low-ionization interstellar absorption lines, which is plotted in red. (right) The visual difference between the two extreme spectra in the left-hand panel is confirmed by the mean $E(B-V)$ for each of the four Ly α quartiles, which decreases as a function of increasing Ly α emission.

population of LBGs as a whole. Narrowband searches are frequently used to probe redshifts higher than $z \sim 3$, so it is important to understand how the properties of narrow-band-selected objects relate to those of general population of star-forming galaxies at similar epochs.

Extending the work of Steidel et al. (2000), we have now measured Ly α equivalent widths for the entire LBG spectroscopic sample.¹⁰ Figure 8 shows the rest-frame $W_{\text{Ly}\alpha}$ distribution, which has a median of ~ 0 \AA and ranges from < -50 \AA in absorption to > 100 \AA in emission. The precise measurement of absorption equivalent widths is difficult, given the broad nature of Ly α absorption, the presence of strong metal absorption lines at nearby wavelengths (Si III $\lambda 1206$ and Si II $\lambda \lambda 1190, 1193$), and the uncertainty in determining the continuum level on the blue side of the line due to Ly α forest absorption. The typical uncertainties in absolute equivalent widths can be larger than $\sim 50\%$ for absorption profiles, while emission equivalent widths are better determined, with $\sim 30\%$ uncertainties. The Ly α profiles for 38% of the galaxies consist of a combination of both emission and absorption. For galaxies characterized by this type of profile, two equivalent widths were measured: a total equivalent width representing the sum of the emission and absorption components, and also an emission equivalent width representing the emission alone. The intrinsic rest-frame UV color, and implied dust extinction, $E(B-V)$, were computed by correcting the observed $G-R$ color for both the total Ly α equivalent width, and also the average IGM absorption along the line of sight.

In order to understand the factors which determine the emergent Ly α profile in LBGs, we binned the sample of 794 individual spectra with Ly α measurements according to $W_{\text{Ly}\alpha}$ into

4 subsamples of equal size. A composite spectrum was constructed from each subsample. The large number of galaxies contained in each bin insured that the resulting composite spectrum had very high S/N, yet there were also enough separate bins that the Ly α properties of the subsamples at each extreme were quite distinct: the bin at one extreme was characterized by objects with strong absorption, while the other extreme bin was dominated by objects with large emission equivalent widths. We obtain several striking results from binning the sample according to $W_{\text{Ly}\alpha}$ and measuring the features of the resulting composite spectra. These measurements are summarized in Table 3.

As shown in Figure 9, the average absorption equivalent width of the 6 strongest low-ionization interstellar lines, W_{LIS} , decreases in strength by almost a factor of three as $W_{\text{Ly}\alpha}$ varies from -15 \AA in absorption to 50 \AA in emission. Even in the spectrum with the strongest Ly α emission and weakest absorption lines, the ratio of Si II $\lambda 1260$ and $\lambda 1526$ absorption equivalent widths is roughly unity. This indicates that the lines are still saturated and that the change in low-ionization equivalent width across the sample is not primarily due to a change in metallicity. There is no significant change in the absorption strength of the high-ionization interstellar absorption lines, W_{SiIV} and W_{CIV} , as $W_{\text{Ly}\alpha}$ varies from strong absorption to strong emission, except in the quartile of galaxies with $W_{\text{Ly}\alpha} \geq 20$ \AA , which has line strengths smaller than the other three quartiles by 50% (still a much less significant change than what is seen in the low ions). Additionally, the Si IV doublet ratio is consistent with the transition being optically thin in all four subsamples.

Another important result is that the UV continuum slope becomes significantly bluer as $W_{\text{Ly}\alpha}$ varies from strong absorption

¹⁰ There are actually 17 galaxies in the spectroscopic sample for which we did not measure the Ly α equivalent width. Most of these galaxies are towards the low-redshift end of the LBG redshift distribution such that Ly α was not contained in the spectral format of the LRIS detector. Additionally there are galaxies for which Ly α fell on top of some defect in the two dimensional spectral image, precluding us from robustly measuring an equivalent width.

to strong emission. This result is most dramatically illustrated by the left-hand box of Figure 10, which shows how the strong-absorption and strong-emission composite spectra, normalized at 1100 Å, diverge at longer wavelengths. To support this visual picture, the right-hand box of Figure 10 shows that the mean $E(B-V)$ value for each of the four subsamples decreases as a function of increasing $W_{\text{Ly}\alpha}$ emission.

Furthermore, Figure 11 shows that with increasing Ly α emission strength, the kinematic offset implied by the relative redshifts of Ly α emission and low-ionization interstellar absorption lines decreases monotonically from $\Delta v_{\text{em-abs}} = 800$ km s $^{-1}$ to $\Delta v_{\text{em-abs}} = 480$ km s $^{-1}$. The kinematic offsets were measured directly from the composite spectra. Weak Ly α emission is detected even in the spectrum composed of the quartile of galaxies with strong absorption and no emission on an individual basis. Therefore, a kinematic offset can be estimated even for this absorption sample.

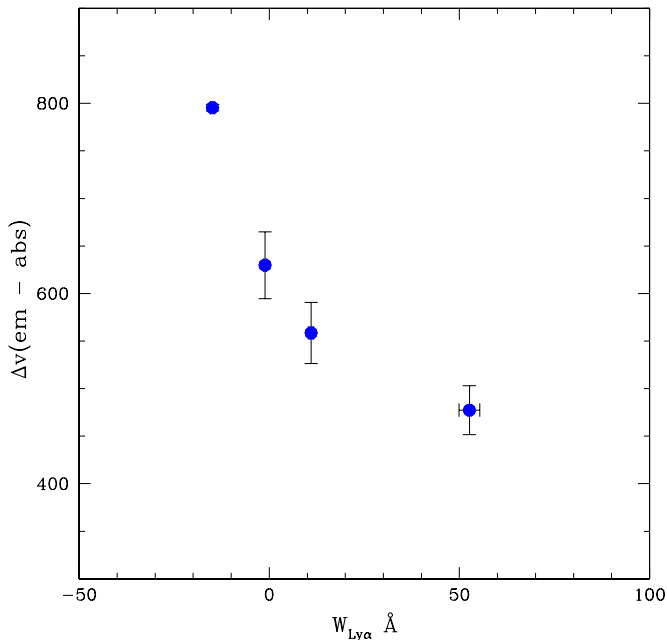


FIG. 11.— The dependence of $\Delta v_{\text{em-abs}}$ on Ly α equivalent width. Velocity offsets between Ly α emission and the strongest low-ionization interstellar absorption lines were measured directly from the composite spectra of each of the four Ly α subsamples. As Ly α emission strength increases, the kinematic offset decreases. The error bars on the velocity offsets represent the scatter among the velocities of the different individual interstellar absorption features.

Now we focus on the composite spectrum of the quartile of galaxies with $W_{\text{Ly}\alpha} \geq 20$ Å, which is strong enough to be selected by current narrow-band emission line search techniques (Hu, Cowie, & McMahon 1998; Rhoads et al. 2000). This composite spectrum has significantly stronger C III] and O III] nebular emission line strengths than the composite spectra with weaker Ly α emission (see Figure 12). In contrast to the strong low-ionization and high-ionization absorption lines, which probe conditions in the foreground, outflowing interstellar medium, the nebular lines act as probes of H II regions where stars are forming. These strength of these features should be independent of conditions in the foreground gas and associated orientation effects, and more sensitive to the nebular temperature and metallicity, and the nature of the stellar population.

The sample with $W_{\text{Ly}\alpha} \geq 20$ Å in emission is much more

complete as a function of \mathcal{R} magnitude than the spectroscopic sample as a whole, since we don’t fail spectroscopically on objects with observed equivalent widths of $W_{\text{Ly}\alpha, \text{obs}} \geq 80$ Å (the same as rest-frame $W_{\text{Ly}\alpha} \geq 20$ Å at $z \sim 3$). Therefore, this sample is ideal to test for the dependence of Ly α emission strength on apparent UV luminosity. We divide the galaxies with $W_{\text{Ly}\alpha} \geq 20$ Å into three groups according to \mathcal{R} magnitude, and compare the three distributions of Ly α equivalent widths. The mean $W_{\text{Ly}\alpha}$ increases towards fainter magnitudes, and a one-dimensional K-S test shows that there is only a 0.1% chance that the brightest distribution of $W_{\text{Ly}\alpha}$ could be drawn from the same parent population as the faintest sample. Since any individual $W_{\text{Ly}\alpha}$ measurement has a significant uncertainty, especially at faint magnitudes, we check this statistical result by constructing composite spectra of the faintest third and brightest third of the subsample with $W_{\text{Ly}\alpha} \geq 20$ Å. Measured directly from the bright and faint composite spectra, which are shown in Figure 13, the Ly α equivalent widths are $W_{\text{Ly}\alpha}(\text{bright}) = 43$ Å and $W_{\text{Ly}\alpha}(\text{faint}) = 65$ Å. Even in the faintest subsample, which has the strongest Ly α emission of any LBG subsample, the average value of $W_{\text{Ly}\alpha}(\text{faint}) = 65$ Å is still well below what is expected for Case B recombination, given a stellar population continuously forming stars with a Salpeter IMF for ≤ 1 Gyr (Charlot & Fall 1993). Therefore, the escape of Lyman continuum photons from LBG star-forming regions is not ruled out by the strength of Ly α emission, and the escape fraction from LBGs is probably determined much more by the covering fraction of outflowing neutral clouds at larger radii (Heckman et al. 2001a; Steidel, Pettini, & Adelberger 2001).

At least in part due to selection effects, the quartile of the sample with the strongest Ly α emission is significantly fainter on average than the quartile with the strongest Ly α absorption. The mean apparent magnitude of the strong absorption quartile is $\mathcal{R} = 24.44$, while the mean apparent magnitude of the strong emission quartile is $\mathcal{R} = 24.85$. Since grouping the sample by $W_{\text{Ly}\alpha}$ also segregates to a certain degree by \mathcal{R} magnitude, it is important to show that the significant spectroscopic trends hold at fixed apparent UV luminosity, especially at an apparent magnitude where all spectroscopic “types” are sampled equally. Therefore, we zero in on the range $\mathcal{R} = 24 - 24.5$, and bin the 207 galaxies in this magnitude range into four equal subsamples according to $W_{\text{Ly}\alpha}$. As shown in Figure 14, the same strong Ly α -dependent trends hold at fixed magnitude: as Ly α changes from strong absorption to strong emission, the average W_{LIS} significantly decreases, and the UV continuum slope becomes significantly bluer; simultaneously, the average W_{SiIV} and W_{CIV} remain roughly independent of $W_{\text{Ly}\alpha}$. The fixed-magnitude Ly α sample is roughly 4 times smaller than the total Ly α sample, and therefore weak nebular emission lines are not detected with much significance. The same significant Ly α -dependent trends are found to apply as well for fixed-magnitude bins of $\mathcal{R} = 24.5 - 25$ and $\mathcal{R} = 25 - 25.5$. LBG photometric and spectroscopic selection effects should not introduce a correlation between $W_{\text{Ly}\alpha}$ and W_{LIS} , or between $W_{\text{Ly}\alpha}$ and UV continuum slope. The consistency of the trends at different \mathcal{R} magnitudes provides direct evidence that magnitude-dependent selection effects have not spuriously introduced correlations; we consider the physical significance of these trends in section 6.

5.4. UV Color Dependences

At $z \sim 3$, the intrinsic UV color, $(G - \mathcal{R})_0$, is determined by correcting the observed $G - \mathcal{R}$ color for the observed Ly α equiv-

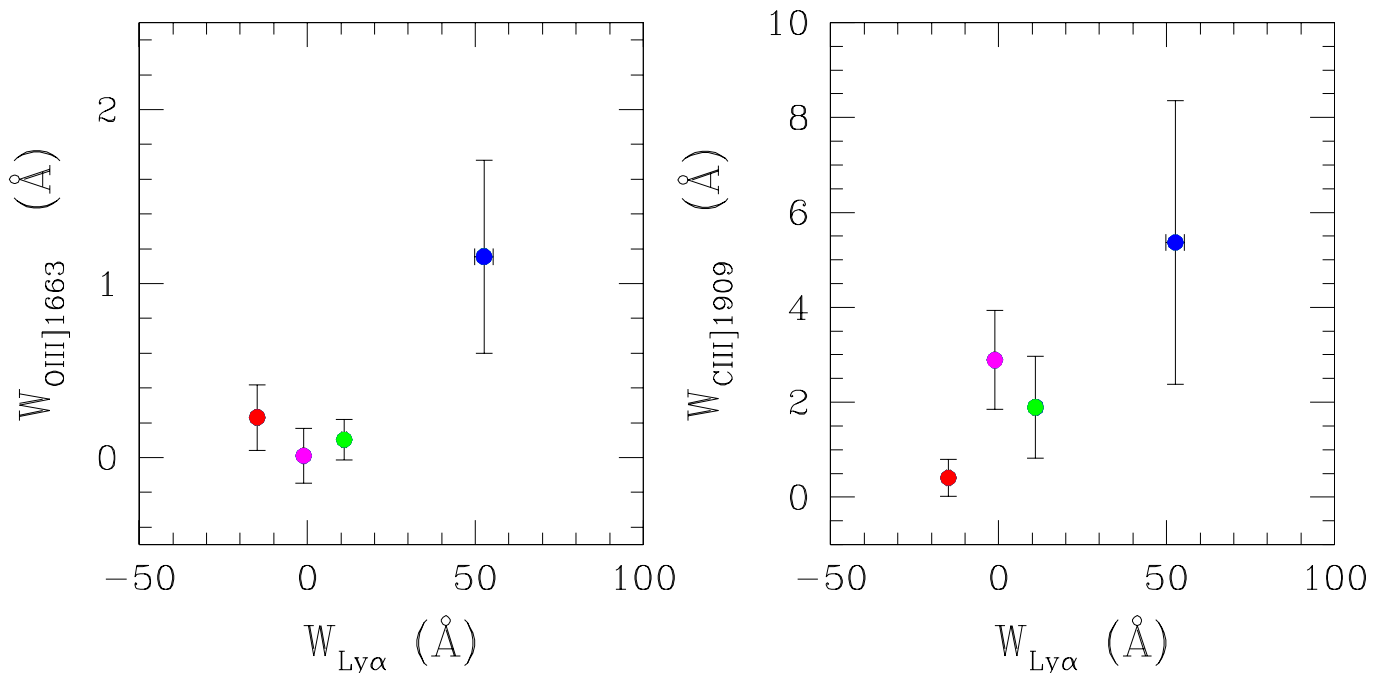


FIG. 12.— The dependence of O III] and C III] nebular emission strength on Ly α equivalent width. The composite spectrum constructed from the quartile of galaxies with $W_{\text{Ly}\alpha} \geq 20 \text{ \AA}$ has significantly stronger nebular emission than the rest of the sample.

alent width, and the redshift-dependent average Ly α forest opacity (Madau 1995). A stellar population continuously forming stars (an appropriate model of the UV colors and spectra of most LBGs) has an unreddened UV spectral energy distribution shape that remains fairly constant for ages between 10 Myr and 1 Gyr.¹¹ Therefore, the range of LBG $(G-\mathcal{R})_0$ colors can be parameterized in terms of $E(B-V)$, the amount of dust extinction reddening the intrinsic UV continuum. In order to convert $(G-\mathcal{R})_0$ to $E(B-V)$, we assume for the unreddened stellar population a 300 Myr old continuous star-formation model – the median age for a subsample of LBGs with optical-IR colors (Shapley et al. 2001). We also assume a relatively grey form for the dust extinction law, which accurately describes the dust properties of local starburst galaxies (Calzetti 1997; Calzetti et al. 2000; Meurer, Heckman, & Calzetti 1999). While the evidence at high redshift is still preliminary, multi-wavelength observations show that the starburst extinction law predicts the properties of LBGs at X-ray and radio wavelengths much better than extinction laws appropriate for the SMC or Ultra-Luminous Infrared Galaxies (ULIRGs) (Seibert, Heckman, & Meurer 2002; Meurer, Heckman, & Calzetti 1999; Nandra et al. 2002).

Based on the range of UV colors of LBGs, and the types of assumptions described above, Adelberger & Steidel (2000) find that the UV luminosities of LBGs are attenuated on average by a factor of ~ 7 due to dust extinction, and that this factor ranges from 0–100. Additionally, LBGs with more dust extinction have higher intrinsic star-formation rates and younger stellar populations (Adelberger & Steidel 2000; Shapley et al. 2001). The role played by star-formation induced outflows in the evolution of the dust properties of LBGs was addressed qualitatively by Shapley et al. (2001), but without the benefit of detailed spectroscopic analysis. Here, we fold in spectroscopic

information to gain a more complete picture of the relationship between dust extinction and outflows.

As presented in section 5.3, when Ly α varies from strong absorption to strong emission: 1) the strength of the low-ionization interstellar absorption lines decreases 2) the dust-sensitive UV continuum becomes bluer. Given the strong interdependence of $W_{\text{Ly}\alpha}$, W_{LIS} , and $E(B-V)$, it is interesting to consider which correlations among the three variables are stronger, and therefore fundamental, and which arise as a by-product of the more fundamental correlations. When the sample is divided into $E(B-V)$ quartiles, we confirm the same interdependence of $W_{\text{Ly}\alpha}$, W_{LIS} , and $E(B-V)$. Figure 15 also demonstrates that W_{LIS} is more strongly dependent on $W_{\text{Ly}\alpha}$ than on $E(B-V)$. Though W_{LIS} becomes significantly weaker (a factor of 1.6) as $E(B-V)$ decreases from the reddest to the bluest quartile, there is a more significant change in W_{LIS} (a factor of 2.7) as $W_{\text{Ly}\alpha}$ varies from strong absorption to strong emission. The variance in W_{LIS} as a function of $E(B-V)$ cannot be accounted for entirely by the change in $W_{\text{Ly}\alpha}$, however; $W_{\text{Ly}\alpha}$ only changes from $W_{\text{Ly}\alpha}(\text{red}) = 5$ to $W_{\text{Ly}\alpha}(\text{blue}) = 20 \text{ \AA}$ as $E(B-V)$ decreases from the reddest to the bluest quartile (in contrast to the change from $W_{\text{Ly}\alpha}(\text{abs}) = -15 \text{ \AA}$ to $W_{\text{Ly}\alpha}(\text{em}) = 50 \text{ \AA}$ in the four Ly α subsamples). According to the relationship between $W_{\text{Ly}\alpha}$ and W_{LIS} presented in section 5.3, we would predict a smaller difference between $W_{\text{LIS}}(\text{red})$ and $W_{\text{LIS}}(\text{blue})$ to accompany the difference between $W_{\text{Ly}\alpha}(\text{red})$ and $W_{\text{Ly}\alpha}(\text{blue})$. We therefore infer a direct statistical link between the absorbing gas and the reddening of the UV continuum, as well as between the absorbing gas and the Ly α profile.

Due to selection effects, the bluest quartile is fainter ($\langle \mathcal{R} \rangle = 24.75$) than the reddest quartile ($\langle \mathcal{R} \rangle = 24.51$). To remove the effects of luminosity, we again examine whether the trends still hold when we look in fixed magnitude ranges: $\mathcal{R} = 24$ –

¹¹ If the spectral energy distribution is parameterized as $F_\lambda \propto \lambda^\beta$, β only ranges between -2.6 and -2.1 for continuous star-formation ages between 10 Myr and 1 Gyr (Leitherer et al. 1999).

24.5, 24.5 – 25, 25 – 25.5. The strength of correlations with $E(B-V)$ is independent of magnitude, though there is a systematic offset in the “zeropoints”, such that galaxies of a given $E(B-V)$ have stronger $\text{Ly}\alpha$ and weaker low-ionization interstellar absorption lines at fainter \mathcal{R} magnitudes. The qualitative similarity of the $E(B-V)$ correlations at all magnitudes confirms their connection to actual physical conditions, rather than to luminosity-dependent selection effects. For LBGs in general, and especially for LBGs in a fixed magnitude range, the dependence of spectroscopic properties on dust extinction is roughly equivalent to the dependence on (slightly model-dependent) dust-corrected star-formation rate. Therefore, galaxies with redder UV continua, stronger interstellar absorption lines, and weaker $\text{Ly}\alpha$ emission, also have larger star-formation rates.

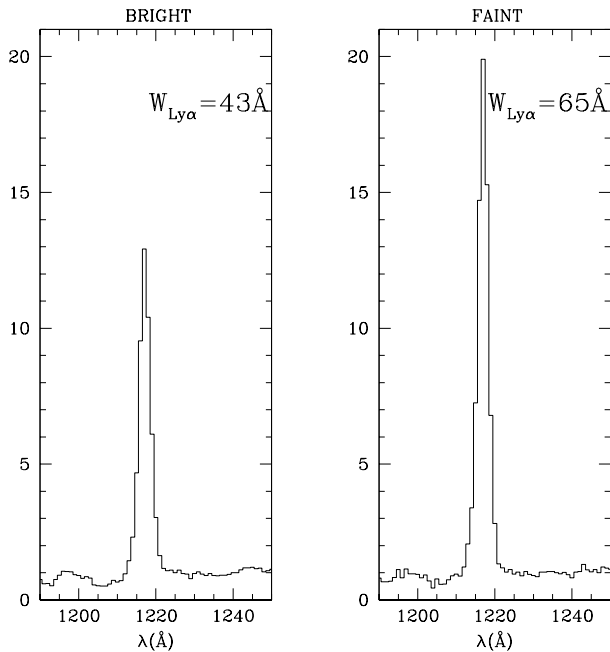


FIG. 13.— The dependence of $W_{\text{Ly}\alpha}$ on apparent UV luminosity. Restricting the comparison to galaxies with $W_{\text{Ly}\alpha} \geq 20 \text{ \AA}$, which should not be prone to magnitude-dependent selection effects, we construct composite spectra for faint (right panel) and bright (left panel) galaxies. Equivalent widths are measured directly from the continuum-normalized composite spectra and indicate that fainter galaxies have larger $\text{Ly}\alpha$ emission equivalent widths than brighter galaxies.

5.5. Kinematic $\Delta v_{\text{em-abs}}$ Dependences

The multi-wavelength properties of “superwinds” in local starburst galaxies have been studied with spatially resolved imaging and spectroscopy (Heckman et al. 2000, 2001b). Also, the hydrodynamics of different phases of the outflowing ISM have been modeled numerically (Strickland & Stevens 2000). Due to their small angular sizes and faint magnitudes, there is very little two-dimensional morphological information or spatially resolved spectroscopy of $z \sim 3$ star-forming galaxies. However, the one dimensional spectroscopic properties of LBGs indicate the presence of large velocity fields, consistent with the outflow conditions seen in local starbursts. In individual spectra, the $\text{Ly}\alpha$ and interstellar redshift differ, with an average offset of $\Delta v_{\text{em-abs}} = 650 \text{ km s}^{-1}$, ranging from less than 0 km s^{-1} to greater than 1000 km s^{-1} (sections 3.1, 4.2, Figure 1). The composite spectrum of the total LBG spectroscopic sample, at rest with respect to stars and H II regions,

has $\Delta v(\text{Ly}\alpha) = +360 \text{ km s}^{-1}$ and $\Delta v(\text{LIS}) = -150 \text{ km s}^{-1}$, implying $\Delta v_{\text{em-abs}} = 510 \text{ km s}^{-1}$. This offset is smaller than the average $\Delta v_{\text{em-abs}}$ measured from individual spectra, but we actually expect the total sample to have a smaller average $\Delta v_{\text{em-abs}}$ than the subsample of objects with both emission and absorption redshifts. This is because the total composite spectrum has stronger $\text{Ly}\alpha$ emission than the composite spectrum constructed only from objects with individual $\Delta v_{\text{em-abs}}$ measurements, and section 5.3 demonstrated a correlation between $W_{\text{Ly}\alpha}$ and $\Delta v_{\text{em-abs}}$.

Since the $\Delta v_{\text{em-abs}}$ distribution for the 323 galaxies with both $\text{Ly}\alpha$ emission and interstellar absorption redshifts is fairly broad, it affords sufficient dynamic range for us to consider how other galaxy properties depend on outflow kinematics. Studies of the radiative transfer of $\text{Ly}\alpha$ in local starburst galaxies (Kunth et al. 1998) stress the importance of ISM kinematics on the emergent $\text{Ly}\alpha$ profile. With our sample, we can directly test the link between $\text{Ly}\alpha$ equivalent width and ISM kinematics. Also, $\Delta v_{\text{em-abs}}$ should be related to the velocity FWHM of the outflowing gas. The FWHM of blue-shifted gas will determine the range of wavelengths of $\text{Ly}\alpha$ photons that are scattered. Blue-shifted gas with a larger velocity dispersion will scatter $\text{Ly}\alpha$ photons with a larger range of wavelengths, pushing the observed centroid of $\text{Ly}\alpha$ emission to longer wavelengths, and causing a larger apparent $\Delta v_{\text{em-abs}}$ for the same outflow velocity (see Figure 3 of Adelberger et al. 2002a). Ideally, we would like to examine the relationship between $\Delta v_{\text{em-abs}}$ and the intrinsic FWHM of the strong low-ionization interstellar absorption lines. We are hampered in this effort by the uncertainty in the effective spectral resolution of our composite spectra. Even when all of the spectra are shifted into the absorption rest frame to minimize the effects of redshift errors, the FWHM measurements are quite noisy and difficult to interpret. However, a comparison between the much better determined W_{LIS} and $\Delta v_{\text{em-abs}}$ may help to isolate the kinematic contribution to the saturated absorption equivalent widths.

The galaxies with $\Delta v_{\text{em-abs}}$ measurements are divided into three subsamples, with $\langle \Delta v_{\text{em-abs}} \rangle = 340, 620, 890 \text{ km s}^{-1}$, and a composite spectrum is constructed for each subsample. Due to the requirement that both emission and absorption features are present in order to compute $\Delta v_{\text{em-abs}}$, the kinematic sample is biased towards brighter objects. However, there should be no biases which prevent us from including certain types of objects as a differential function of $\Delta v_{\text{em-abs}}$. Consistent with the results of section 5.3, we find that $W_{\text{Ly}\alpha}$ weakly dependent on $\Delta v_{\text{em-abs}}$ (Figure 16). While statistically significant, the difference between $W_{\text{Ly}\alpha}(\Delta v = 340)$ and $W_{\text{Ly}\alpha}(\Delta v = 890)$ is small compared to the large range of $W_{\text{Ly}\alpha}$ seen in the entire sample. Also, W_{LIS} marginally increases with increasing $\Delta v_{\text{em-abs}}$, though the difference is not significant, and may arise as a result of the strong correlation between $\text{Ly}\alpha$ and the interstellar absorption lines (Figure 16). Somewhat surprisingly, the sample with $\langle \Delta v_{\text{em-abs}} \rangle = 890 \text{ km s}^{-1}$ has very strong *high*-ionization equivalent widths, though the Si IV doublet ratio indicates that Si IV is still optically thin. Relative to the average values for the total LBG sample (section 4.2.2), the high Δv sample has $W_{\text{Si IV}}$ and $W_{\text{C IV}}$ that are 50% higher. Finally, the UV continuum becomes bluer with increasing velocity width (Figure 16). None of the correlations with $\Delta v_{\text{em-abs}}$ is as significant as the trends among $W_{\text{Ly}\alpha}$, W_{LIS} , and $E(B-V)$.

5.6. Comparison with Local Starburst Results

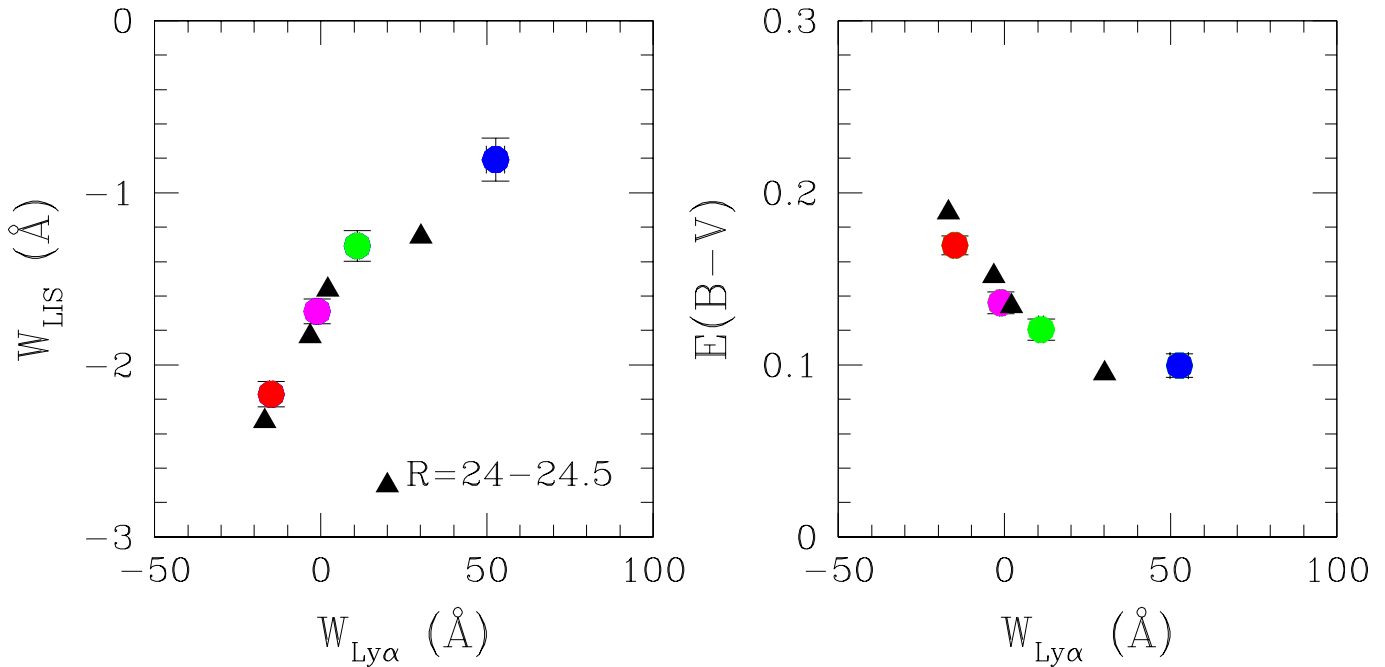


FIG. 14.— Strong Ly α -dependent trends at fixed \mathcal{R} magnitude. Galaxies with $\mathcal{R} = 24-24.5$ are divided into four subsamples based on Ly α equivalent width, and black triangles indicate measurements from the corresponding composite spectra. **Left:** W_{LIS} vs. $W_{\text{Ly}\alpha}$. Colored symbols are as in Figure 9. Galaxies with $\mathcal{R} = 24-24.5$ follow the same trend as the total sample. **Right:** $E(B-V)$ vs. $W_{\text{Ly}\alpha}$. Colored symbols are as in Figure 10, and galaxies with $\mathcal{R} = 24-24.5$ obey the same correlation.

A systematic analysis of the UV spectroscopic properties of local starburst galaxies was carried out by Heckman et al. (1998), intended to guide the interpretation of UV spectroscopic properties of high-redshift star-forming galaxies. Several starburst parameters were considered, including UV continuum slope, UV and bolometric luminosity, UV low-ionization interstellar equivalent width, high-ionization stellar wind equivalent width, and nebular metallicity. One of the parameters carrying a lot of the variance of the properties of local starbursts is metallicity, measured from the nebular oxygen abundance, O/H. More metal-rich starbursts have more dust extinction, higher star-formation rates, and stronger UV absorption lines. Since there are nebular O/H measurements for only a handful of LBGs, and the C/O measurements from the composite spectra are very uncertain, it is not possible to make a direct comparison to the metallicity-dependent results for local starbursts. Moreover, a large part of the analysis in the present work addresses the factors which control the emergent Ly α profile in LBGs, which is, ironically, much harder to study at low redshift due to contamination from geocoronal Ly α , and therefore not included in the Heckman et al. analysis. However, we can directly compare the local and high-redshift results for the relationship between UV continuum reddening and interstellar absorption line strengths. Both in local starbursts and LBGs, there is a strong correlation between W_{LIS} and UV continuum reddening. Since the absorption lines are saturated in both samples, variations in their equivalent widths reflect changes in the combination of neutral gas covering fraction and velocity dispersion, rather than in metal abundance. For the local starbursts, the correlation is interpreted as resulting from the mutual dependence of both W_{LIS} and dust extinction on the velocity dispersion of the absorbing neutral gas. As described more fully in section 6.1, we offer a different interpretation of this trend.

We can compare the $z \sim 3$ results about Ly α emission with other local studies. In contrast to the apparent decoupling be-

tween Ly α extinction and continuum reddening found in local starburst galaxies (Giavalisco, Koratkar, & Calzetti 1996a) we find a significant correlation between UV continuum extinction and $W_{\text{Ly}\alpha}$. Either this difference between the local starbursts and LBGs points to a significant difference between the geometries of dusty neutral gas in star-forming galaxies at low and high-redshift, or else the low-redshift sample suffered from the vagaries of small sample statistics. In the work of Kunth et al. (1998), strong Ly α absorption is seen in cases where the interstellar absorption lines are static with respect to the galaxy systemic velocity, whereas Ly α emission is detected in galaxies with blue-shifted interstellar absorption lines. The blue-shift of interstellar absorption lines is ubiquitous in the LBG spectroscopic sample, even in galaxies with strong Ly α absorption. In contrast to the evidence at low redshift, the presence of an outflow in LBGs is not a sufficient criterion for detecting Ly α emission. In fact, it appears that the Ly α emission equivalent width *increases* as the velocity offset between Ly α and the interstellar absorption lines decreases.

In local starbursts, the UV nebular emission lines such as C III] $\lambda 1909$ are stronger in starbursts of lower metallicity (Heckman et al. 1998). This effect is most likely due to a decrease in the nebular electron temperature of higher metallicity gas, which causes more of the nebular cooling from collisionally excited lines to occur in the infrared rather than the UV. Collisionally excited C III] and O III] nebular emission lines are stronger than average in the composite spectrum of LBGs with $W_{\text{Ly}\alpha} \geq 20 \text{ \AA}$. By analogy with the local results, this subsample may be composed of objects with lower than average LBG metallicities. The C/O ratio in the strong emission composite spectrum implies an O/H abundance which is lower than the average O/H observed in the small sample of LBGs with rest-frame optical spectroscopic measurements (Pettini et al. 2001), though the uncertainties in both measurements are

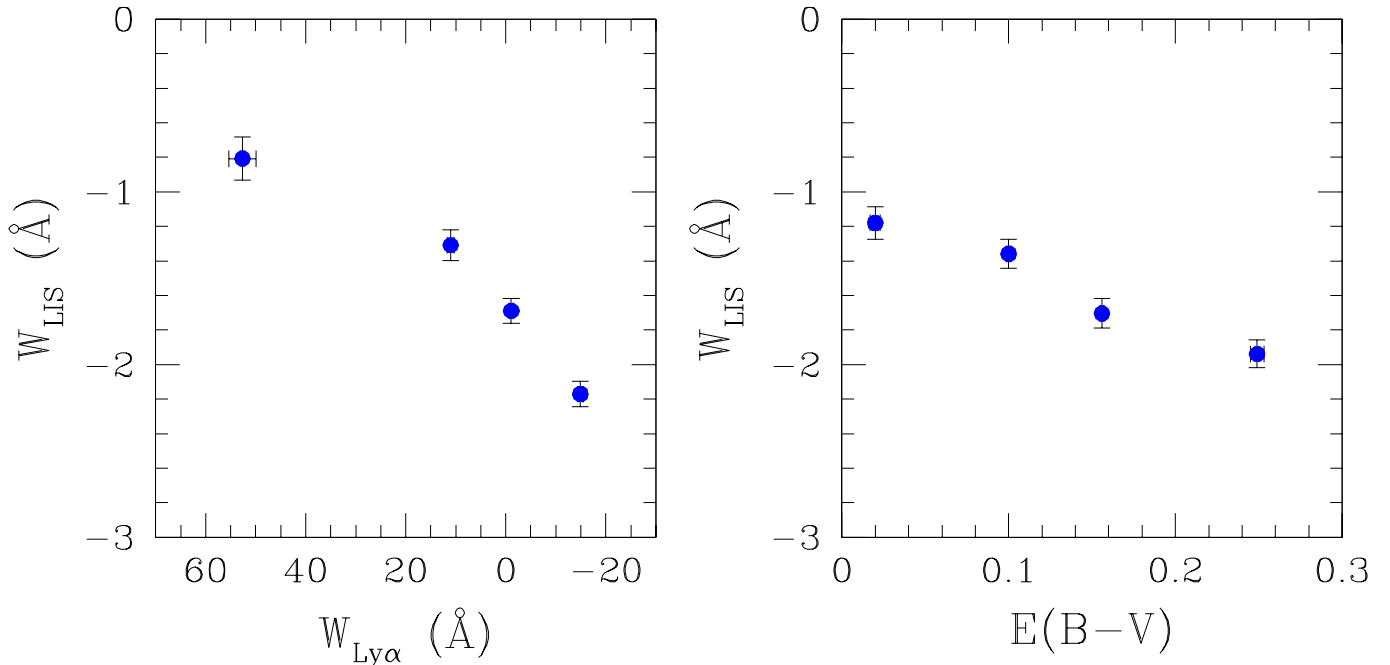


FIG. 15.— The dependence of low-ionization interstellar absorption strength, W_{LIS} , on both $\text{Ly}\alpha$ equivalent width and dust reddening. These plots show the results of dividing LBG spectroscopic sample into quartiles, according to either $\text{Ly}\alpha$ equivalent width (left) or $E(B-V)$ (right). While W_{LIS} depends strongly on both $W_{\text{Ly}\alpha}$ and $E(B-V)$, there is more variance in W_{LIS} when the sample is sorted by $W_{\text{Ly}\alpha}$. This suggests a stronger statistical link between W_{LIS} and $W_{\text{Ly}\alpha}$, though the correlation between W_{LIS} and $E(B-V)$ is strong enough that there may be a direct physical connection among all three quantities.

large. Important future observations include nebular metallicity measurements of statistical samples of LBGs, when multi-object rest-frame optical spectroscopy becomes possible. Also important are outflow metallicity measurements from unsaturated interstellar absorption lines, which will be possible with higher S/N and resolution rest-frame UV spectra.

6. SUMMARY AND DISCUSSION

We have presented a summary of the spectroscopic features contained in LBG rest-frame UV spectra, and the important trends among UV continuum reddening; outflow kinematics; and the equivalent widths of $\text{Ly}\alpha$, low- and high-ionization interstellar absorption, and nebular emission. The most important results are:

1. LBGs with stronger $\text{Ly}\alpha$ emission have bluer UV continua, weaker low-ionization interstellar absorption lines, smaller kinematic offsets between $\text{Ly}\alpha$ emission and interstellar absorption lines, and lower star-formation rates (the last property may be due in part to selection effects).

2. Low- and high-ionization absorption equivalent widths exhibit different behaviors as functions of other spectral properties.

3. Galaxies with rest-frame $W_{\text{Ly}\alpha} \geq 20 \text{ \AA}$ in emission have weaker than average high-ionization lines, and nebular emission lines which are significantly stronger than in the rest of the sample. In the subsample with strong emission lines, which is itself fainter than average for the spectroscopic sample, there is evidence that $\text{Ly}\alpha$ emission strength increases towards fainter magnitudes (and lower star-formation rates). To study the dependence of the full distribution of $\text{Ly}\alpha$ equivalent widths on luminosity, a more careful treatment of photometric and spectroscopic incompleteness is required.

6.1. A Physical Picture

Ultimately, these spectroscopic trends are not very interesting unless we consider what they imply about the physical conditions in LBGs and their outflows. Here we offer a picture which is consistent with all of the observations, and highlight empirical results which still require further explanation. In high-resolution optical and near-IR images, LBGs have typical half-light radii of $1.6h^{-1}$ kpc (Giavalisco, Steidel, & Macchetto 1996b). This typical half-light radius represents the scale of the H II regions where massive star formation takes place. The UV stellar continuum, photospheric and wind features, and UV and optical nebular emission lines are produced here. Negligible systemic velocities of nebular emission lines with respect to stellar photospheric absorption features indicate that the massive stars and H II regions are at rest with respect to each other (sections 3.1 and 4.3.2). Also produced in the H II regions through recombinations of ionized hydrogen are the original $\text{Ly}\alpha$ photons which subsequently diffuse through frequency space and through dusty neutral gas at larger radii.

A generic feature of galaxies selected with Lyman Break color criteria is a star-formation surface density high enough that the mechanical energy input from the resulting large number of Type II supernova explosions drives a large bubble of hot gas out of the galaxy (Heckman 2002). This superbubble expands at several hundred km s^{-1} , and may eventually escape the galactic gravitational potential, possibly without radiating away most of the mechanical energy input from supernovae (Adelberger 2002a). The location, relative to the central star-formation regions, of the neutral and ionized gas giving rise to strong blueshifted absorption is an important component of any physical picture describing the spectra of LBGs.

Neutral gas displays a range of blue-shifted line-of-sight velocities with an average of $\Delta v \sim -200 \text{ km s}^{-1}$, but extending to $\Delta v \sim -600 \text{ km s}^{-1}$ (Pettini et al. 2002). If cold neutral interstellar clouds are entrained and accelerated by the flow of

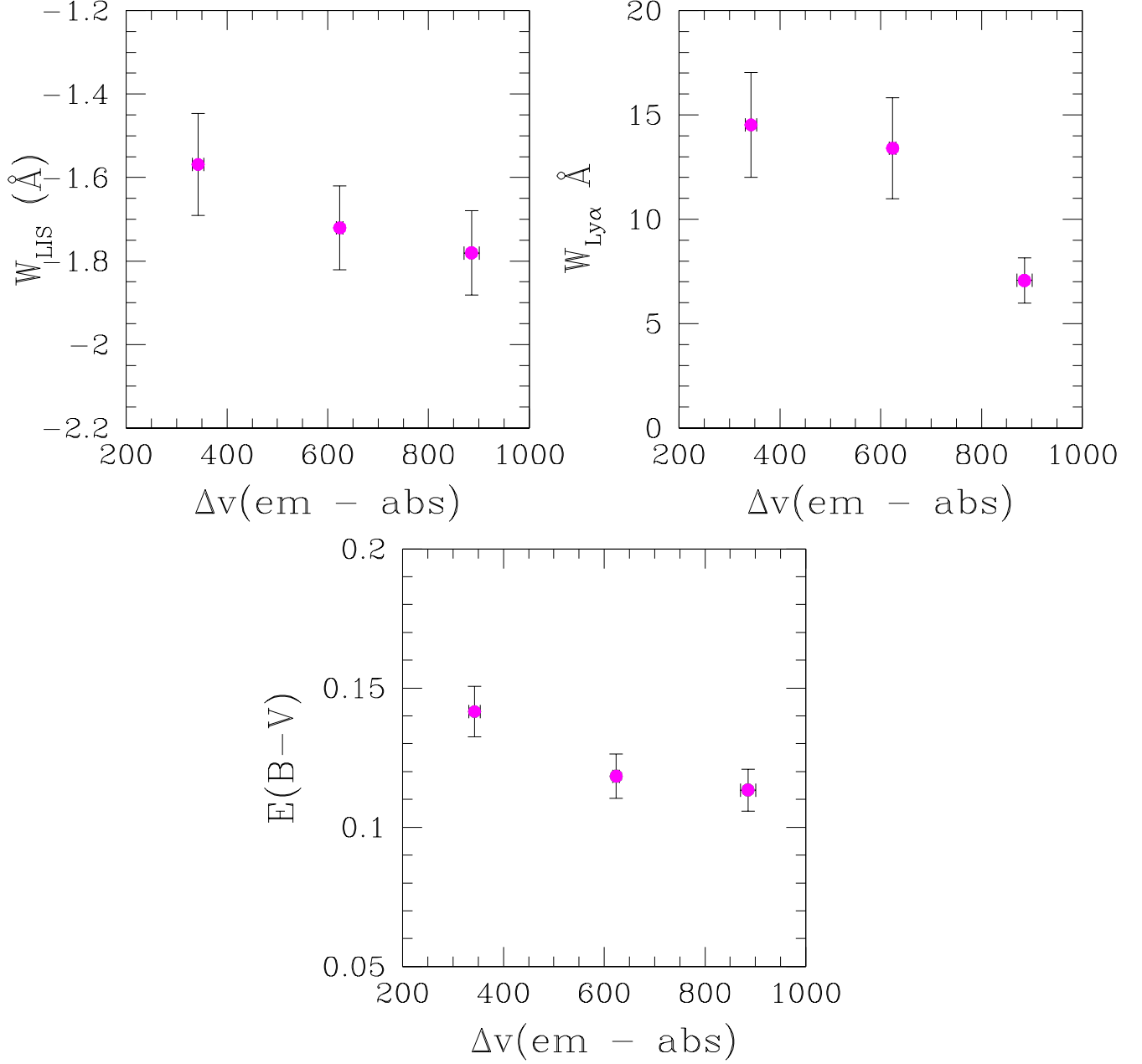


FIG. 16.— Dependences of W_{LIS} , $W_{\text{Ly}\alpha}$, and $E(B-V)$ on $\Delta v_{\text{em-abs}}$. These plots show the average W_{LIS} , $W_{\text{Ly}\alpha}$, and $E(B-V)$ values measured from each of the 3 subsets of galaxies sorted by $\Delta v_{\text{em-abs}}$, and their associated composite spectra. W_{LIS} and $E(B-V)$ are not significantly dependent on Δv , while $W_{\text{Ly}\alpha}$ is smaller for the subsample with the highest Δv ($\geq 800 \text{ km s}^{-1}$). This trend is consistent with the fact that the Δv measured in the composite spectrum with the strongest Ly α absorption is larger than the Δv measured in the spectrum with the strongest Ly α emission. However, the change in $W_{\text{Ly}\alpha}$ with Δv is small compared with the total variance of Ly α across the whole LBG spectroscopic sample.

hot gas, they may reside at smaller distances, r , than the expanding shock front of the superbubble. A plausible lower limit to r is the typical LBG half-light radius, $1.6h^{-1}$ kpc, given that the majority of LBG rest-frame UV spectra exhibit such strong absorption lines. If the absorbing gas were at much smaller radii, more mixed in with the stars, we would expect a much smaller covering factor, and weaker absorption on average. An upper limit on r may be obtained from consideration of close pairs of LBGs, by searching for absorption from the lower redshift member of a pair in the spectrum of the higher redshift one. There are 17 LBG pairs with projected separations of $r_\theta < 160h^{-1}$ comoving kpc. When the spectra of the higher-redshift pair members are shifted into the rest-frame of the lower-redshift galaxies and averaged, little Ly α or metal absorption is detected. The mean impact parameter in these pairs is $110h^{-1}$ kpc, which puts an upper limit of $r \lesssim 25h^{-1}$ proper kpc on the physical dimensions of the gas giving rise to strong blue-shifted absorption in LBG spectra (Adelberger et al. 2002a).

Along with neutral material, there is also ionized gas with a similar mean blueshift and range of velocities over which absorption takes place. Blue-shifted Si IV and C IV absorption features are produced in this gas, which has been ionized by a mixture of radiation and collisional processes. In contrast to the low-ionization features, the Si IV doublet appears to be optically thin. While the neutral and ionized phases have comparable kinematic properties, this similarity does not necessarily constrain their relative physical distributions. In alternate scenarios consistent with the kinematics of the low and high ions, 1) the Si IV and C IV absorption may be produced in the outer ionized regions of the outflowing clouds giving rise to low-ionization absorption, or 2) it may originate in more diffuse, but still outflowing, ionized gas in which the outflowing neutral clouds are embedded. There may also be evidence for a third, hotter phase of gas at $T \sim 3 \times 10^5$ K, if the O VI producing absorption is collisionally ionized. In the future, it will be interesting to compare the kinematics of the O VI absorption with that of the low-ions and other high-ions, using higher spectral resolution data.

Heckman et al. (2001b) and Strickland & Stevens (2000) have considered the outflow scenario in detail for local starbursts, and Adelberger (2002a) and Pettini et al. (2002) have done the same for LBGs at $z \sim 3$. The composite LBG spectra provide some new results about outflows at high redshift. The low-ionization interstellar absorption lines are the most direct probe of the outflowing neutral gas, and there is clearly a direct link between W_{LIS} and the emergent Ly α profile. Quite strikingly, the interstellar absorption strength monotonically decreases as the Ly α emission strength increases. Also important is the decoupling of the behavior of neutral and ionized absorbing gas. When the sample is divided according to $W_{\text{Ly}\alpha}$, W_{LIS} varies by almost a factor of three, whereas W_{SiIV} stays roughly constant except for the sample with strong Ly α emission, in which the high-ions are 50% weaker. The difference between the behavior in low and high ion line strengths is especially intriguing since the two sets of lines have similar mean blue-shifts and velocity FWHMs. This result may be evidence for a variable neutral gas covering fraction in the outflow, whereas the ionized gas maintains a more constant covering fraction. It also favors the scenario in which patchy neutral clouds are embedded in an ionized gas phase with unity covering fraction, rather than the one in which Si IV and C IV absorption are produced

in the outer regions of the patchy neutral clouds.

Dust has been observed in the outflows from local star-forming galaxies (Heckman et al. 2000). In this work, we also find strong evidence for dust in the outflowing neutral clouds at $z \sim 3$. The correlation between the W_{LIS} and $E(B-V)$ is most naturally explained if some fraction of the reddening of the stellar continuum takes place in the outflowing gas. The strong correlation between W_{LIS} and $E(B-V)$ also argues for an outflow geometry which is at least comparable in size to the galaxy half-light radii – i.e. the absorbing neutral clouds must be distributed in front of the entire face of the galaxy, affecting the total region of UV continuum surface brightness, and not only a small central region. LBGs differ from local galaxies hosting starbursts in terms of two important geometrical properties, which may also distinguish the nature and evolution of LBG outflows from local ones. First, local starbursts often occur in a central nuclear region with $r_* \leq 1$ kpc, which is small compared to the galaxy half-light radius, whereas LBGs indicate high star-formation surface-densities over a larger size-scale. Second, local star-forming galaxies often have large gas disks. Superwinds expand perpendicular to these disks, in the direction of the steepest pressure gradient (Heckman et al. 2000; Heckman 2002). Based on the morphological information about LBGs and models of galaxy formation, such disks were probably not in place at $z \sim 3$.

6.2. The Absorbing Gas

The properties of the blue-shifted neutral gas are crucial in determining the appearance of LBG rest-frame UV spectra. The equivalent widths of these low-ionization lines correlate strongly with two key spectroscopic properties: $W_{\text{Ly}\alpha}$ and $E(B-V)$. An important question is: what physical parameter of the low-ionization gas governs the equivalent widths? As stated before, the four strongest low-ionization lines must be saturated based on the ratio of equivalent widths of different Si II transitions. Therefore, the change in average equivalent width by a factor of ~ 3 reflects a change in the neutral clouds' velocity dispersion, covering fraction, or both. Using all of the available information, we attempt to infer which of these properties is reflected by the change in W_{LIS} .

Since W_{LIS} is so strongly correlated with $W_{\text{Ly}\alpha}$, we focus on the properties of the composite spectra described in section 5.3, constructed from subsamples sorted by $W_{\text{Ly}\alpha}$. This is, for practical purposes, equivalent to sorting by W_{LIS} , which we would like to do, but cannot, given the quality of the individual spectra. The relevant measurements are the observed residual intensities and FWHMs of the low-ionization interstellar absorption lines. For saturated lines, the deconvolved residual intensity is an empirical estimate of the gas covering fraction, (i.e. $I = 1 - C_f$, where I is the residual intensity, and C_f is the covering fraction). The observed residual intensities smoothly increase as $W_{\text{Ly}\alpha}$ increases from strong absorption to strong emission (Figure 9). Also, the observed FWHMs of the composite spectrum with the strongest Ly α emission are narrower than those in the strongest absorption composite, though there is not a smooth trend with $W_{\text{Ly}\alpha}$.

Ideally, we would like to determine simultaneously the deconvolved FWHMs and residual intensities of the low-ionization interstellar absorption lines. The deconvolved quantities depend very sensitively on the effective spectral resolutions of the four Ly α composite spectra, however, and these four spectral resolutions may not even be equivalent. For exam-

ple, spectra with Ly α emission could have been spectroscopically identified under conditions of worse atmospheric seeing than absorption-only spectra. Another effect is that the systemic redshift formulae from Adelberger et al. (2002a) have different levels of precision for different types of spectra. The effective spectral resolution is only constrained to be between $\Delta\lambda \sim 2.0\text{--}3.2 \text{ \AA}$ for the four spectra, which is of the same order as the intrinsic FWHMs. When the spectral resolution is so uncertain, yet comparable to the intrinsic FWHMs, resolution effects are degenerate with both intrinsic FWHM and residual intensity. Thus, we can only say that there is a significant reduction in the *product* of covering fraction and velocity spread as the absorption lines decrease in equivalent width,

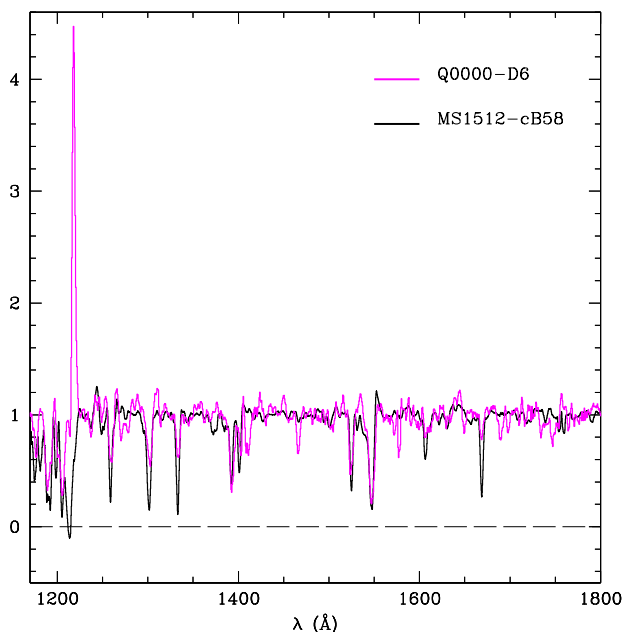


FIG. 17.— Continuum-normalized spectra of the two highest S/N LBGs in the spectroscopic sample: MS1512-cB58 and Q0000-D6. cB58 (plotted in black) belongs in the quartile of LBGs with the strongest Ly α absorption, while Q0000-D6 (plotted in magenta) is in the 30% of the sample with the strongest Ly α emission. The contrast between Ly α profiles is clear, as is the contrast between W_{LIS} absorption strengths. On the other hand, the strength of the high-ionization absorption lines is roughly comparable. In this case, where we know the spectral resolution accurately for both spectra, we can show that the intrinsic velocity widths of the absorption lines are comparable, and that the difference in W_{LIS} between cB58 and Q0000-D6 is due to a difference in the covering fraction of neutral gas.

Without a quantitative determination of the relative significance of velocity FWHM and covering fraction in moderating W_{LIS} , we offer two pieces of circumstantial evidence that covering fraction may be the more important effect of the two. First, we compare the spectroscopic properties of the two brightest spectroscopically confirmed LBGs that are not AGN: MS1512-cB58 ($\mathcal{R} = 20.6$) and Q0000-D6 ($\mathcal{R} = 22.88$). cB58 is in the quartile of LBGs with the strongest Ly α and low-ionization interstellar absorption. In contrast, Q0000-D6 has $W_{\text{Ly}\alpha}$ and W_{LIS} which place it in the second highest quartile of $W_{\text{Ly}\alpha}$ emission. As shown in Figure 17, the difference in Ly α properties of the two objects is reflected in the difference in low-ionization equivalent widths, which are ~ 1.6 times stronger in cB58 than in Q0000-D6 (though, just as in the composite spectra, the high-ionization line-strengths are roughly the same strength). In this case, we explicitly measure the velocity widths of the

low-ionization lines in cB58 and Q0000-D6. The C II $\lambda 1334$ FWHM is measured directly from the high-resolution spectrum of cB58 as $\text{FWHM}(\text{cB58}) = 655 \text{ km s}^{-1}$. Based on a careful analysis of the spatial extent of the object along the slit in the 2D spectrogram of the low-resolution spectrum of Q0000-D6, we estimate a rest-frame resolution of $\Delta\lambda = 2.5 \text{ \AA}$ and the deconvolved C II $\lambda 1334$ velocity width is $\text{FWHM}(\text{D6}) = 665 \text{ km s}^{-1}$. In this case, cB58 and Q0000-D6 have the same low-ionization velocity dispersions, and the difference in equivalent width can only be explained as a difference in the covering fraction of blueshifted neutral clouds. While the cB58 C II line has a residual intensity of ~ 0 , implying a unity covering fraction, the intrinsic residual intensity in Q0000-D6 is 0.4, implying a covering fraction of only 60%. The second piece of circumstantial evidence is the strong correlation between W_{LIS} and $E(B-V)$ (sections 5.3 and 5.4). Heckman et al. (1998) attribute this correlation in local starbursts to the fact that the velocity dispersion in the absorbing gas must be larger in galaxies with more dust extinction. This explanation is plausible in that galaxies with higher star-formation rates can drive winds with larger velocity spreads (Heckman et al. 2000), and they are also dustier (Adelberger & Steidel 2000; Shapley et al. 2001). However, a more direct explanation for the correlation results if the blue-shifted neutral gas is dusty. Accordingly, galaxies with a larger covering fraction of dusty clouds suffer more extinction of the UV stellar continuum, as well as exhibiting larger saturated equivalent widths, and weaker Ly α emission.

6.3. Lyman Continuum Leakage

One of the reasons we have devoted so much of the discussion to the covering fraction of neutral gas is that this property may determine how optically thick LBGs are to their own H I-ionizing radiation. The optical depth of LBGs to Lyman continuum photons is a cosmologically interesting question, given the controversy surrounding the contribution of galaxies to the ionizing background at $z \sim 3$. Escaping Lyman continuum flux was apparently detected by Steidel, Pettini, & Adelberger (2001) in a composite spectrum of 29 LBGs drawn from the high-redshift tail of the current spectroscopic sample. This spectrum is very similar to the composite spectrum of the total LBG spectroscopic sample (Figure 2) in terms of $W_{\text{Ly}\alpha}$, W_{LIS} and W_{HIS} , though it indicates less reddening by dust ($\langle E(B-V) \rangle = 0.07$ for the galaxies in the Lyman continuum sample, and $\langle E(B-V) \rangle = 0.13$ for galaxies in the total LBG sample). As discussed before, the composite spectrum of the total LBG sample suffers from its own selection biases with respect to the LBG UV luminosity function. Therefore, the similarity of the Lyman continuum composite spectrum to the total LBG composite spectrum is not proof that the Lyman continuum spectrum represents a true “average” $z \sim 3.4$ galaxy spectrum.

Furthermore, in contradiction to the apparent detection of Lyman continuum emission, Giallongo et al. (2002) derive an upper limit for the escape fraction in two bright LBGs which is four times lower than Steidel et al (2001) detection. One of these two galaxies is Q0000-D6, (section 6.2), which apparently has only 60% covering fraction of gas capable of producing significant low-ionization metal absorption lines! If there are indeed no unresolved saturated components in the low-ionization features which are missed due to finite spectral resolution, the case of Q0000-D6 may imply that low-ionization lines which do not reach zero intensity are a necessary but not sufficient condition for the escape of Lyman continuum emis-

sion. For example, we note that the cores of the high-ionization lines in the spectrum of Q0000-D6 are black (when viewed at sufficient spectral resolution using the Keck Echelle Spectrograph and Imager). If these transitions arise in gas with sufficient neutral hydrogen column density to be optically thick to Lyman continuum photons, very little ionizing radiation will escape from Q0000-D6. It is clearly of great interest to push the Lyman continuum observations of this galaxy to more sensitive limits than those achieved so far.

In order to arrive at the global contribution of LBGs to the ionizing background, high-resolution spectra are necessary to measure the neutral gas velocity dispersions and covering fractions without degeneracy as a function of $W_{\text{Ly}\alpha}$, W_{LIS} , W_{HIS} , $E(B-V)$, and $\Delta v_{\text{em-abs}}$. Once it is understood how the gas covering fraction depends on other spectroscopic parameters, we need to construct an unbiased estimate of the average spectrum of the light associated with LBGs. Proper weighting of each individual spectrum as a function of its \mathcal{R} magnitude and Ly α equivalent width should compensate for all of the photometric and spectroscopic biases presented in section 5.1 yielding the true average spectrum. Based on the spectroscopic properties of the average spectrum, the average LBG neutral gas covering fraction can be inferred. The final step is to use direct observations of the Lyman continuum region to calibrate the relationship between gas covering fraction and Lyman continuum leakage. If it is possible to calibrate this relationship, the average LBG covering fraction can be converted into a true average Lyman continuum escape fraction.

6.4. Future Observations

While this work has illuminated the range of rest-frame UV spectroscopic properties of LBGs, there are many limitations in the data which prevented us from drawing quantitative conclusions, and which highlight the need for several specific future observations. Data of higher spectral resolution are necessary to measure the velocity distribution and covering fraction of the absorbing neutral gas without degeneracy. Properties such as stellar population age should be folded into the analysis to search for temporal evolution in the UV spectroscopic properties. Comparing the *HST* morphologies of galaxies of different spectroscopic types will also aid in understanding the effects of geometry and orientation. With such observations we will truly be able to characterize the detailed effects of star-formation at $z \sim 3$, both on galaxies and the intergalactic medium.

We wish to extend special thanks to those of Hawaiian ancestry on whose sacred mountain we are privileged to be guests. Without their generous hospitality, most of the observations presented herein would not have been possible. We also thank Mark Dickinson, Mauro Giavalisco, Mindy Kellogg, Matthew Hunt, and Dawn Erb, who assisted in the observations and reductions, and the referee, Claus Leitherer for careful and helpful suggestions which improved the quality of the paper. CCS and AES have been supported by grant AST-0070773 from the U.S. National Science Foundation and by the David and Lucile Packard Foundation. KLA acknowledges support from the Harvard Society of Fellows.

REFERENCES

- Adelberger, K. L. 2002a, ApJ, submitted
 Adelberger, K. L. 2002b, Ph. D. Thesis
 Adelberger, K. L. & Steidel, C. C. 2000, ApJ, 544:218
 Adelberger, K. L., Steidel, C. C., Giavalisco, M., Dickinson, M. E., Pettini, M., & Kellogg, M. 1998, ApJ, 505, 18
 Adelberger, K. L., Steidel, C. C., Shapley, A. E., & Pettini, M. 2002a, ApJ, in press
 Adelberger, K. L., Steidel, C. C., Shapley, A. E., & Pettini, M. 2002b, ApJ, submitted
 Allende Prieto, C., Lambert, D. L., & Asplund, M. 2002, ApJ, 573, L137
 Bahcall J. N. & Wolf R. A. 1968, ApJ, 152, 701
 Bruhweiler, F. C., Kondo, Y., McCluskey, G. E. 1981, ApJS, 46, 255
 Calzetti, D. 1997, AJ, 113, 162
 Calzetti, D., Armus, L., Bohlin, R. C., Kinney, A. L., Koornneef, J., & Storchi-Bergmann, T. 2000, ApJ, 533, 682
 Carigi, L. 2000, RMxAA, 36, 171
 Charlot, S., & Fall, S. M. 1993, ApJ, 415, 580
 Chen, W. L., & Neufeld, D. A. 1994, ApJ, 432, 567
 Conti, P. S., Leitherer, C., & Vacca, W. D. 1996, ApJ, 461, L87
 Cowie, L. L., & Hu, E. M. 1998, AJ, 115, 1319
 de Mello, D. F., Leitherer, C., & Heckman, T. M. 2000, ApJ, 530, 251
 Ferland, G. J., Korista, K. T., Verner, D. A., Ferguson, J. W., Kingdon, J. B. & Verner, E. M. 1998, PASP, 110, 761
 Ferland, G. J., & Osterbrock, D. E. 1986, ApJ, 300, 658
 Franx, M., Illingworth, G. D., Kelson, D. D., van Dokkum, P. G., Tran, K.-V. 1997, ApJ, 486, L75
 Garnett, D. R., Shields, G. A., Peimbert, M., Torres-Peimbert, S., Skillman, E. D., Dufour, R. J., Terlevich, E., & Terlevich, R. J. 1999, ApJ, 513, 168
 Garnett, D. R., Skillman, E. D., Dufour, R. J., Peimbert, M., Torres-Peimbert, S., Terlevich, R. J., Terlevich, E., & Shields, G. A. 1995, ApJ, 443, 64
 Garnett, D. R., Skillman, E. D., Dufour, R. J., & Shields, G. A. 1997, ApJ, 481, 174
 Giallongo, E., Cristiani, S., D'Odorico, S., Fontana, A. 2002, ApJ, 568, L9
 Giavalisco, M., Koratkar, A., & Calzetti, D. 1996a ApJ, 466, 831
 Giavalisco, M., Steidel, C. C., Adelberger, K. L., Dickinson, M. E., Pettini, M., & Kellogg, M. 1998, ApJ, 503, 543
 Giavalisco, M., Steidel, C. C., & Macchetto, F. D. 1996b, ApJ, 470, 189
 Gonzalez Delgado, R. M., Leitherer, C., Heckman, T. M., Lowenthal, J. D., Ferguson, H. C., & Robert, C. 1998, ApJ, 495, 698
 Groenewegen, M. A. T., Lamers, H. J. G. L. M., Pauldrach, A. W. A. 1989, A&A, 221, 78
 Haehnelt, M. G., Madau, P., Kudritzki, R., Haardt, F. 2001, ApJ, 549, L151
 Hartmann, L. W., Huchra, J. P., & Geller, M. J. 1984, ApJ, 287, 487
 Hartmann, L. W., Huchra, J. P., Geller, M. J., O'Brien, P., & Wilson, R. 1988, ApJ, 326, 101
 Heckman, T. M. 2002, in ASP Conf. Ser. 254, Extragalactic Gas at Low Redshift, ed. J. Mulchaey & J. Stocke (San Francisco: ASP), 292
 Heckman, T. M., Lehnert, M. D., Strickland, D. K., Armus, L. 2000, ApJS, 129, 493
 Heckman, T. M., Robert, C., Leitherer, C., Garnett, D. R., & van der Rydt, F. 1998, ApJ, 503, 646
 Heckman, T. M.; Sembach, K. R., Meurer, G. R., Leitherer, C., Calzetti, D., Martin, C. L. 2001a, ApJ, 558, 56
 Heckman, T. M., Sembach, K. R., Meurer, G. R., Strickland, D. K., Martin, C. L., Calzetti, D., Leitherer, C. 2001b, ApJ, 554, 1021
 Holweber, H. 2001, in AIP Conf. Proc. 598, Solar and Galactic Composition, ed. R. F. Wimmer-Schweingruber (Melville, NY: AIP), 23
 Hu, E. M., Cowie, L. L., & McMahon, R. G. 1998, ApJ, 502, L99
 Keenan, F. P., Cook, J. W., Dufton, P. L., Kingston, A. E. 1992, ApJ, 387, 726
 Kinney, A. L., Bohlin, R. C., Calzetti, D., Panagia, N., & Wyse, R. F. G. 1993, ApJS, 86, 5
 Kobulnicky, H. A., & Skillman, E. D. 1998, ApJ, 497, 601
 Kunth, D., Lequeux, J., Sargent, W. L. W., & Viallefond, F. 1994, A&A, 282, 709
 Kunth, D., Mas-Hesse, J. M., Terlevich, E., Terlevich, R., Lequeux, J., & Fall, S. M. 1998, A&A, 334, 11
 Leitherer, C., Leao, J. R. S., Heckman, T. M., Lennon, D. J., Pettini, M., & Robert, C. 2001, ApJ, 550, 724
 Leitherer, C., Robert, C., Heckman, T. M. 1995, ApJS, 99, 173
 Leitherer, C., et al. 1999, ApJS, 123, 3
 Leitherer, C., Vacca, W. D., Conti, P. S., Filippenko, A. V., Robert, C., & W. L. W. Sargent 1996, ApJ, 465, 717
 Lequeux, J., Kunth, D., Mas-Hesse, J. M., & Sargent, W. L. W. 1995, A&A, 301, 18
 Lowenthal, J. D., Koo, D., Guzman, R., Gallego, J., Phillips, A., Faber, S. M., Vogt, N. P., Illingworth, G., & Gronwall, C. 1997, ApJ, 481, 673
 McCarthy, J. K. et al. , "Blue channel of the Keck low-resolution imaging spectrometer," in *Optical Astronomical Instrumentation*, S. D'Odorico, ed., Proc. SPIE, **3355**, pp. 81–92, 1998
 Madau, P. 1995, ApJ, 444, 18
 Maeder, A. 1991, A&A, 242, 93
 Maeder, A. 1992, A&A, 264, 105

- Meier, D., & Terlevich, R. 1981, *ApJ*, 246, L109
- Meurer, G. R., Heckman, T. M., & Calzetti, D. 1999, *ApJ*, 521, 64
- Meynet, G. 1995, *A&A*, 298, 767
- Morris S. L., Weymann R. J., Foltz C. B., Turnshek D. A., Sheckman S., Price C., Boroson T. A. 1986, *ApJ*, 310, 40
- Nandra, K., Mushotzky, R. F., Arnaud, K., Steidel, C. C., Adelberger, K. L., Gardner, J. P., Teplitz, H. I., Windhorst, R. A. 2002, *ApJ*, 576, 625
- Neufeld, D. A. 1990, *ApJ*, 350, 216
- Oke, J. B., et al. 1995, *PASP*, 107, 375
- Papovich, C., Dickinson, M., & Ferguson, H. C. 2001, *ApJ*, 559, 620
- Pettini, M. 2002, in *Cosmochemistry: The Melting Pot of Elements*, (Cambridge: Cambridge University Press), in press (<http://www.ast.cam.ac.uk/~pettini/canaries13/>)
- Pettini, M., Rix, S. A., Steidel, C. C., Adelberger, K. L., Hunt, M. P., & Shapley A. E. 2002, *ApJ*, 569, 742
- Pettini, M., Shapley, A. E., Steidel, C. C., Cuby, J.-G., Dickinson, M. E., Moorwood, A., Adelberger, K. L., & Giavalisco, M. 2001, *ApJ*, 554, 981
- Pettini, M., Steidel, C. C., Adelberger, K. L., Dickinson, M., & Giavalisco, M. 2000, *ApJ*, 528, 96
- Robert, C., Leitherer, C., Heckman, T. M. 1993, *ApJ*, 418, 749
- Rhoads, J. E., Malhotra, S., Dey, A., Stern, D., Spinrad, H. & Januzzi, B. T. 2000, *ApJ*, 545, L85
- Schaerer, D. & Vacca, W. D. 1998, *ApJ*, 497, 618
- Seibert, M., Heckman, T. M., Meurer, G. R. 2002, *AJ*, 124, 46
- Shapley, A. E., Steidel, C. C., Adelberger, K. L., Dickinson, M., Giavalisco, M., & Pettini, M. 2001, *ApJ*, 562, 95
- Shull, J. M. & van Steenberg, M. 1982, *ApJS*, 48, 95
- Steidel, C. C., Adelberger, K. L., Dickinson, M. E., Giavalisco, M., Pettini, M. & Kellogg, M. 1998, *ApJ*, 492, 428
- Steidel, C. C., Adelberger, K. L., Giavalisco, M., Dickinson, M. E., & Pettini, M. 1999, *ApJ*, 519, 1
- Steidel, C. C., Adelberger, K. L., Shapley, A. E., Pettini, M., Dickinson, M., & Giavalisco, M. 2000, *ApJ*, 532, 170
- Steidel, C. C., Giavalisco, M., Dickinson, M., & Adelberger, K. L. 1996a, *AJ*, 112, 352
- Steidel, C. C., Giavalisco, M., Pettini, M., Dickinson, M., & Adelberger, K. L. 1996b, *ApJ*, 462, L17
- Steidel, C. C., Hunt, M. P., Shapley, A. E., Adelberger, K. L., Pettini, M., Dickinson, M., Giavalisco, M. 2002, *ApJ*, 576, 653
- Steidel, C. C., Pettini, M., & Adelberger, K. L. 2001, *ApJ*, 546, 665
- Strickland, D. K., & Stevens, I. R. 2000, *MNRAS*, 314, 511
- Tenorio-Tagle, G., Silich, S. A., Kunth, D., Terlevich, E., & Terlevich, R. 1999, *MNRAS*, 309, 332
- Walborn, N. R., Panek, R. J. 1984, *ApJ*, 280, 27
- Wolfe, A. M., & Prochaska, J. X. 2000a, *ApJ*, 545, 591
- Yee, H. K. C., Ellingson, E., Bechtold, J., Carlberg, R. G., & Cuillandre, J.-C. 1996, *AJ*, 111, 1783

TABLE 1
STRONG LBG INTERSTELLAR ABSORPTION FEATURES

Ion	$\lambda_{\text{lab}}^{\text{a}}$ (Å)	f^{b}	W_0^{c} (Å)	σ^{c} (Å)	Δv^{d} (km s ⁻¹)
Si II	1260.4221	1.007	-1.63	0.10	-110
O I	1302.1685	0.04887	-2.20 ^e	0.12 ^e	[-270] ^e
Si II	1304.3702	0.094	-2.20 ^e	0.12 ^e	[-270] ^e
C II	1334.5323	0.1278	-1.72	0.11	-150
Si IV	1393.76018	0.5140	-1.83	0.16	-180
Si IV	1402.77291	0.2553	-0.81	0.10	-180
Si II	1526.70698	0.130	-1.72	0.18	-110
C IV	1548.204	0.1908	-3.03 ^f	0.21 ^f	[-390] ^f
C IV	1550.781	0.09522	-3.03 ^f	0.21 ^f	[-390] ^f
Fe II	1608.45085	0.058	-0.91	0.15	-60
Al II	1670.7886	1.833	-1.04	0.15	-100

^aVacuum wavelengths.

^bTransition oscillator strengths as in Pettini et al. (2002).

^cRest frame equivalent width and 1σ error. The error takes into account both sample variance and the S/N of the composite spectrum (see section 5.2).

^dRelative velocity measured in the systemic rest frame of the composite spectrum, equivalent to the rest frame of the stars.

^e W_0 , σ , and Δv values listed for O I $\lambda 1302$ and Si II $\lambda 1304$ refer to the total measured for the blend of these two features. The value of Δv assumes that the rest wavelength of the blend is $\lambda = 1303.2694$ Å.

^f W_0 , σ , and Δv values listed for both members of the C IV $\lambda 1548, 1550$ doublet refer to the blend of these two features. There may be a contribution to W_0 from stellar wind absorption which has not been subtracted out. The value of Δv assumes that the rest wavelength of the blend is $\lambda = 1549.479$ Å.

TABLE 2
WEAK LBG EMISSION FEATURES

Ion	$\lambda_{\text{lab}}^{\text{a}}$ (\AA)	A_{ul}^{b} (10^8s^{-1})	W_0^{c} (\AA)	σ^{c} (\AA)	Δv^{d} (km s^{-1})
Si II*	1264.738	2.30e+01	0.34	0.09	+130
Si II*	1309.276	7.00e+00	0.35	0.10	+50
Si II*	1533.431	7.40e+00	0.21	0.09	+110
O III]	1660.809	2.20e-06	0.23 ^e	0.13 ^e	+40
O III]	1666.150	5.48e-06	0.23 ^e	0.13 ^e	-50
CIII]	1908.734	1.14e-06	1.67	0.59	+40

^aVacuum wavelengths.

^bEinstein A -coefficients from the NIST Atomic Spectra Database (http://physics.nist.gov/cgi-bin/AtData/main_asd).

^cRest frame equivalent width and 1σ error. The error takes into account both sample variance and the S/N of the composite spectrum (see section 5.2).

^dRelative velocity measured in the systemic rest frame of the composite spectrum, equivalent to the rest frame of the stars.

^e W_0 and σ values are given for the flux integrated over the whole O III] doublet.

TABLE 3
SPECTROSCOPIC PROPERTIES OF LY α SUBSAMPLES

	Group 1 ^a	Group 2 ^a	Group 3 ^a	Group 4 ^a
N_{gal}	199	198	199	198
$W_{Ly\alpha}$ ^b	-14.92 ± 0.56	-1.10 ± 0.38	11.00 ± 0.71	52.63 ± 2.74
$W_{SiII,1260}$ ^b	-1.85 ± 0.16	-1.59 ± 0.16	-1.36 ± 0.19	-1.05 ± 0.22
$W_{OI+SiII,1303}$ ^b	-3.24 ± 0.16	-2.71 ± 0.16	-1.98 ± 0.19	-1.21 ± 0.21
$W_{CII,1334}$ ^b	-2.34 ± 0.16	-1.91 ± 0.15	-1.43 ± 0.19	-0.83 ± 0.23
$W_{SiII,1526}$ ^b	-2.38 ± 0.19	-1.82 ± 0.19	-1.33 ± 0.23	-1.21 ± 0.33
$W_{FeII,1608}$ ^b	-1.57 ± 0.21	-1.03 ± 0.18	-0.69 ± 0.25	-0.59 ± 0.34
$W_{AlII,1670}$ ^b	-1.64 ± 0.22	-1.08 ± 0.20	-1.07 ± 0.25	0.04 ± 0.44
$W_{SiIV,1393}$ ^b	-1.83 ± 0.23	-1.87 ± 0.21	-1.93 ± 0.27	-1.22 ± 0.30
$W_{SiIV,1402}$ ^b	-1.01 ± 0.17	-0.98 ± 0.16	-0.75 ± 0.21	-0.54 ± 0.23
$W_{CIV,1549}$ ^b	-3.56 ± 0.30	-2.97 ± 0.32	-3.22 ± 0.39	-2.43 ± 0.47
$W_{OIII,1663}$ ^b	0.23 ± 0.19	0.01 ± 0.16	0.10 ± 0.12	1.16 ± 0.56
$W_{CIII,1909}$ ^b	0.41 ± 0.39	2.89 ± 1.04	1.90 ± 1.07	5.37 ± 2.99
$E(B-V)$ ^c	0.169 ± 0.006	0.136 ± 0.006	0.120 ± 0.006	0.099 ± 0.007
β ^c	-0.73 ± 0.03	-0.88 ± 0.04	-0.98 ± 0.03	-1.09 ± 0.05
Δv_{em-abs} (km s ⁻¹)	795 ± 3	630 ± 35	560 ± 30	475 ± 25
\mathcal{R}_{AB}	24.44 ± 0.04	24.49 ± 0.04	24.64 ± 0.04	24.85 ± 0.04
SFR_0 ($h^{-2}M_{\odot} \text{ yr}^{-1}$) ^d	52 ± 5	38 ± 2	29 ± 3	25 ± 3

^aGroups 1 – 4 are the four quartiles of the LBG spectroscopic sample, divided according to Ly α equivalent width.

^bRest-frame equivalent width in \AA , measured from the composite spectra. Positive values indicate emission, while negative values indicate absorption. Uncertainties are calculated as described in section 5.2.

^cEstimates of reddening, based on the intrinsic UV color, $(G-\mathcal{R})_0$. $E(B-V)$ assumes the Calzetti law for dust extinction, and an underlying stellar population with 300 Myr of constant star-formation. β is derived directly from the $(G-\mathcal{R})_0$ color, assuming that the UV spectrum can be described by the form, $F_{\lambda} \propto \lambda^{\beta}$.

^dDust-corrected star-formation rate, derived from the apparent \mathcal{R} magnitude, the redshift, and the amount of UV extinction inferred from the $(G-\mathcal{R})_0$ color.